Doctoral Dissertation

EFFECT OF FIBER WAVINESS ON TENSILE STRENGTH OF A FLAX FIBER-REINFORCED COMPOSITE

(亜麻繊維強化複合材料の引張強度に及ぼす繊維うねりの影響)

September 2015

TAWEESAK PIYATUCHSANANON

Graduate School of Science and Engineering,

Yamaguchi University

Table of contents

Nomenclature

GFRP	Glass fiber-reinforced plastics
FRP	Fiber-reinforced polymer matrix composites
FEM	Finite element method
CFRP	Carbon fiber-reinforced plastics
SLM	Sheet lamination method

Symbols

W_f	Flax fibre weight in the composite
ρ_m	Biodegradable resin density (Mg/m^3)
τ	Shear modulus (MPa)
σ	Tensile strength (MPa)

Chapter I General introduction

1.1 Background

Strong demand for the use of composite materials is increasing today because high strength and stiffness, as well as low density are needed to reduce energy consumption in aviation and automotive transport industries. The use of artificial fiber-reinforced composite materials, such as glass fiber-reinforced plastics (GFRP) and carbon fiber-reinforced plastics (CFRP) is effective to meet these demands, but disposal difficulties that arise after their use has surfaced as an environmental problem. Therefore, many researchers have strived to develop biodegradable renewable composite materials and various production methods for the materials that will widen their practical availability [1-5]. Plant-based natural fibers such as flax, hemp, ramie, jute, kenaf, curaua and bamboo, are expected for use as the composite reinforcement materials, but these are often used as short fibers, as seen in injection-molded products. Long fibers are generally known to be exhibit load-bearing potential in a matrix material as compared to short fibers. Before spinning process, plant-based natural fibers are often supplied as long fibers called 'slivers'. When this form is successfully prepared with resin, slivers can be applied as a semi-finished composite material in prepregs [5, 6]. One of the problems in preparing slivers is their fiber waviness, which is fluctuation in the fiber orientation inherent in plant-based natural fibers as well as synthetic fibers. Such waviness often engenders a decrease in the mechanical properties of the composites. It was pointed out in the model proposed by Hsiao and Daniel [7] that the decrease in elastic properties of a unidirectional carbon/epoxy composite resulted from the fiber waviness. Karami and Garnich [8] used a finite element micromechanical model to predict the effects of periodic and localized fiber waviness on carbon fiber reinforcement. In

these papers, however, the fiber waviness was assumed as a deterministic shape such as a sine curve. In order to take the stochastic wavy effect of sliver into account, Ren et al. [9, 10] quantified the fibre orientation fluctuation in curaua-sliver and flax-sliver-reinforced composite through one-dimensional and two-dimensional autocorrelations between fiber orientation angles on the composite surface. The quantified parameter expressing the degree of the fluctuation, called the "area ratio", was correlated with the composite tensile strength. However, the use of autocorrelations was intended to evaluate the quality of fiber orientation, but not to express the degree of local disorder in fiber orientation. In general, stiffness is insensible for structural defects, but strength is sensible. Therefore, the local disorder in fiber orientation is of great interest for quantification through some statistical or stochastic analytical method. It is also expected that the quantified parameter shall play a role as a key indicator during quality inspection for produced prepregs.

Thus, the purpose of this study is to examine the effects of the fiber waviness on the tensile strength of a flax-sliver-reinforced composite (in-plane tensile modulus). Resin-pasted flax slivers were first compression-molded, and then fiber orientation angles were measured on the surfaces of the resultant composite laminates. To quantify the degree of the disorder in fiber orientation, the measurement results were analyzed by Local Moran's I and Local Geary's c [11], which are measures of the representative spatial autocorrelation analyses. Quantification by the "area ratio" was optimized by seeking an appropriate threshold level of the measures, correlated closely with tensile strength data.

1.1.1 Fiber waviness of a flax sliver-reinforced composite material

Fiber-reinforced polymer matrix composites (FRP) have been used wildly due to the high strength and low specific gravity. However, most of FRP are composed of fiberglass or carbon fibers, of which recycling method or disposal process has not been established yet. While such artificial renewable processes are studied, recently, researchers have tried to use environmental-friendly fibers such as kenaf, ramie and flax as reinforcement, but a problem of using natural fiber is the fiber waviness. Fiber waviness is the fluctuation in fiber orientation, inherent in plant-based natural fibers, that affects the mechanical properties.

Flax slivers (Teikokusen-I Co, Ltd), one of the representative natural fibers, was used as reinforcement, as show in Fig.1.1, and a biodegradable resin (Randy PL-1000; Miyoshi Oil and Fat Co. Ltd., Japan) as a matrix. The resin was supplied in a water emulsion containing micro-order fine particles of approximately 5.0 μm diameter. The Randy PL-1000 is made from plant-derived biodegradable resins. Thus, the resultant composite may be called the 'fully green composite'. Typical physical and mechanical properties of these constituents are shown in table 1. 1

Table 1.1 Properties of the fibers and matrix

Material	Density (Mg/m^3)	Fiber width (μm)	Tensile strength (MPa)	Fracture strain (%)	Young's modulus (GPa)
Randy PL-1000	1.2	-	32.5	-	3.8
Flax fiber	1.50	10-30	600-1100	1.5-2.4	40-100

Fig.1.1 Flax sliver

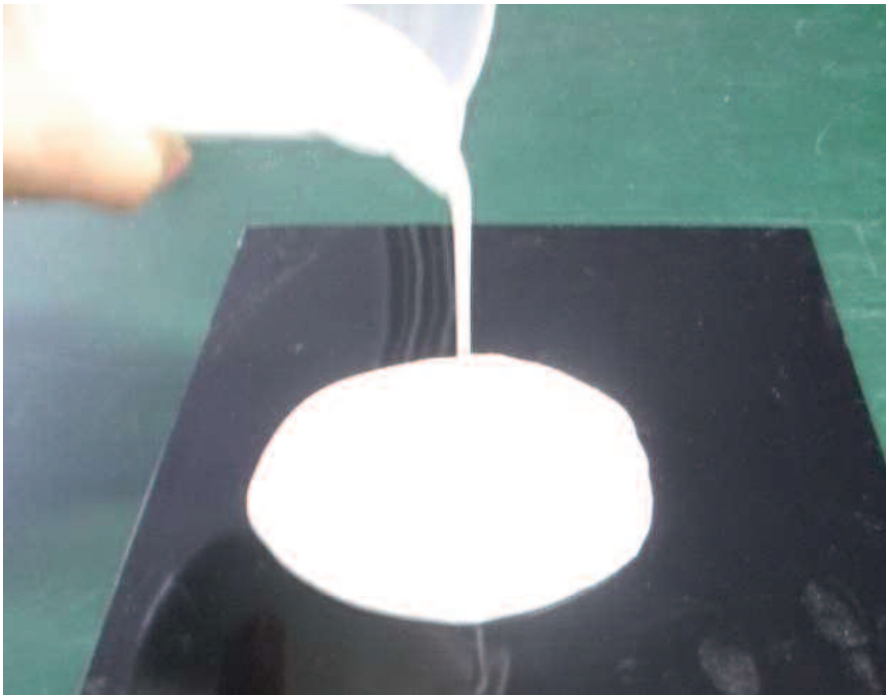

Fig.1.2 A biodegradable resin

1.1.2 Pearson method

Pearson method is a method to analyze point patterns by using the notion of covariance and correlation between two data group. The equation of Pearson method is shown as:

$$\rho_{i,i+k} = \frac{Cov(\Theta_i, \Theta_{i+k})}{\sqrt{Var(\Theta_i)}\sqrt{Var(\Theta_{i+k})}}$$

where Θ_i and Θ_{i+k} respectively denote sets of measured segment angles on i-th and $(i+k)$-th unit composites, and k is the distance between two unit composites. $Cov(\cdot)$ is the autocovariance between two unit composites, and $Var(\cdot)$ is the variance on each unit composite. In Fig.1.3, the correlation between two blocks is calculated at τ_1 and τ_2. τ_1 is a distance between x_i and x_j and τ_2 is distance between y_i and y_i, thus the sizes of τ_1 and τ_2 are 25 and 8 respectively.

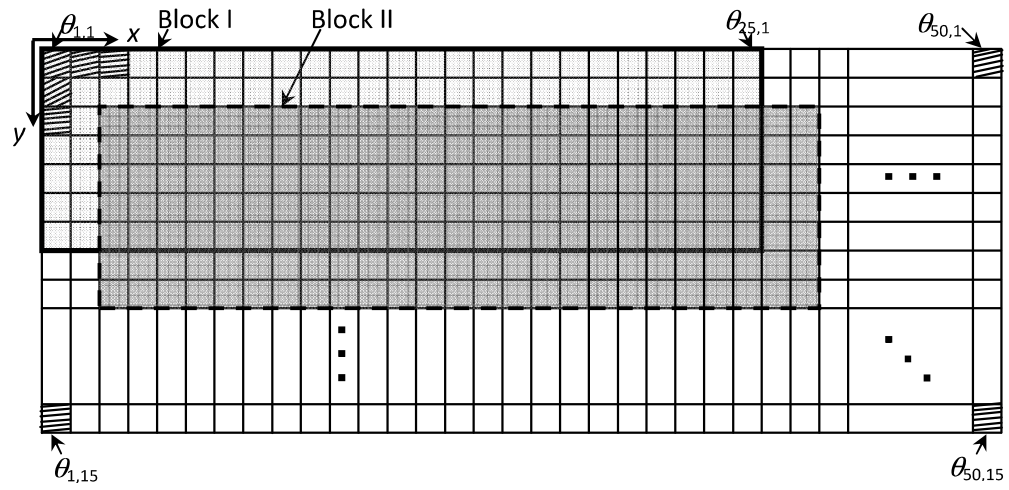

Fig.1.3 Schematic of two-dimensional autocorrelations

The coefficient of Pearson method varies between -1 to +1. The positive coefficient means the value at this location is similar to the neighbor locations, thus the fiber orientation

angle is smoother than the results at the low coefficient. Considering the negative coefficient, the value at that location is similar to the neighbor locations; however it displays a different sign from other locations. The results of Pearson method are shown in fig 1.4.

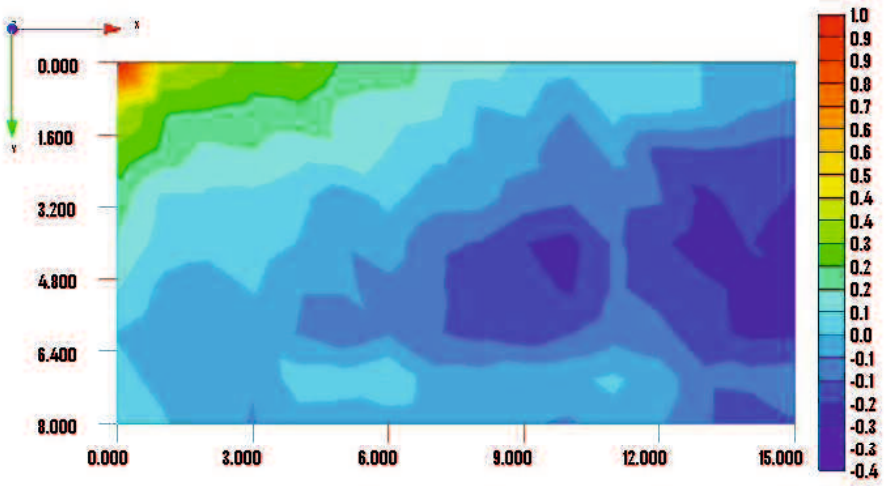

Fig.1.4(a) Pearson method's result of specimen no.1A

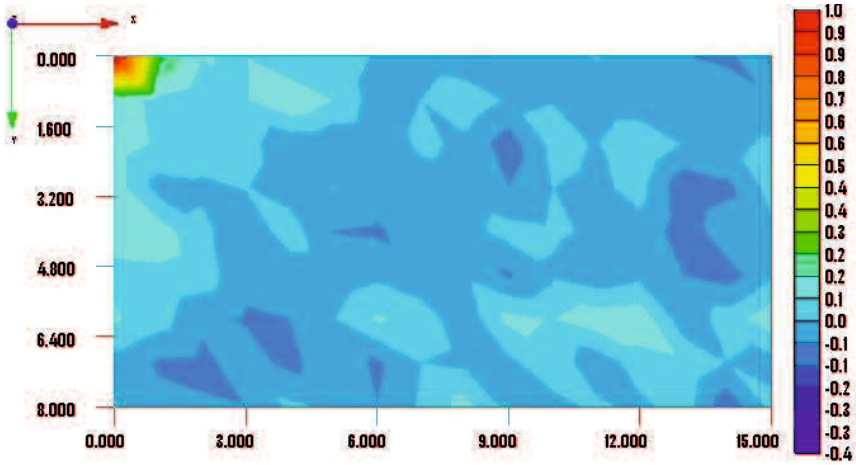

Fig.1.4(b) Pearson method's result of specimen no.7B

As Pearson method's results, they trend toward the negative side more than the positive side. The black areas in fig.1.5 consist of the coefficient higher than 0.3 which is calculated as *R* more than 0.5. The percentage of area ratio is 1% for specimen no.1A and 0.2% for specimen no. 7A. After that, the correlation between area ratio and tensile strength was analyzed for predicting the impact of tensile strength on the specimens. The results of area ratio are shown in fig 1.6

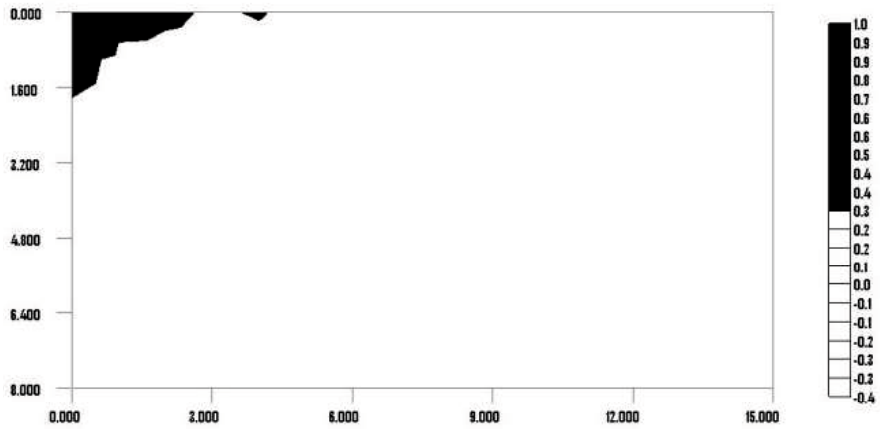

Fig.1.5(a) Contour maps of Pearson's Method 1A

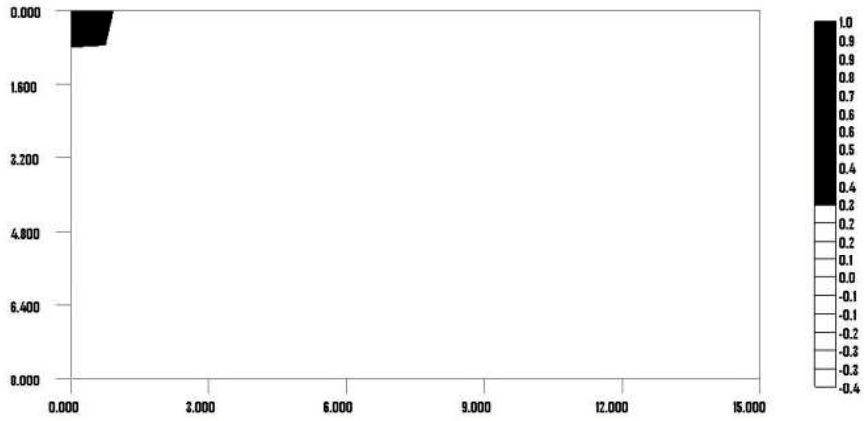

Fig.1.5(b) Contour maps of Pearson's Method 7A

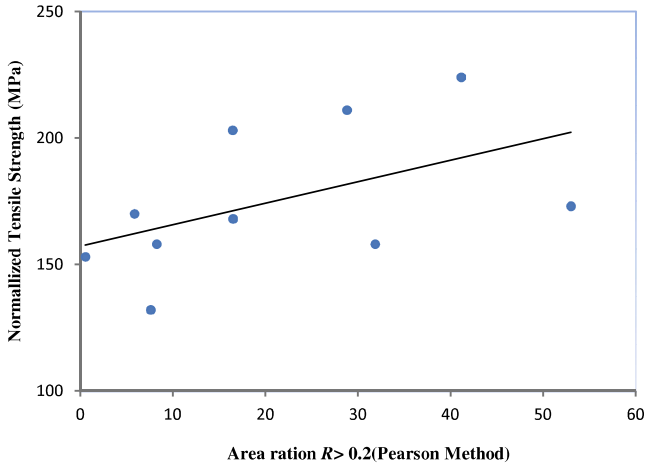

Fig.1.6 (a) Area Ratio dependence on normal tensile strength of Pearson's Method

In this study, we used the correlation method to define the relation between the area ratio of Pearson Method. The correlation between the tensile strength and the area ratio of Pearson Method (>0.3) is higher than 0.5(0.65), which indicates a positive linear relationship. Thus, it is able to determine the relationship between Pearson Method and tensile strength.

1.2 Objectives and outline

In the previous study, the effect of Fiber waviness of a flax sliver-reinforced composite material was analyzed by Pearson method, spatial autocorrelation method in Chapter 1. Pearson method is a method to analyze point patterns by using the notion of covariance and correlation between two data group. Thus, fiber orientation angles are important data for analyzing the effect of fiber waviness. To evaluate the effect of fiber waviness, the area ratio and tensile strength was analyzed. The correlation between the tensile strength and the area ratio of Pearson Method (>0.5) is higher than 0.5, which indicates a positive linear relationship. Thus, it is able to determine the relationship between Pearson Method and tensile strength.

In the present study, the effect of fiber waviness was analyzed by Local Morn's *I*, Local Geary's *c* and Tsai-Hill criteria. This is another method to improve the results of analysis because Local Moran's *I*, Local Geary's *c* and Tsai-Hill criteria have results at each element. Thus, we are able to understand the behavior of the fiber waviness on specimens.

In the chapter II, the object is to examine the effects of the fiber waviness on the tensile strength of a flax-sliver reinforced composite (in-plane tensile modulus). Resin pasted flax slivers were first compression molded, and then fiber orientation angles were measured on the surfaces of the resultant composite laminates. To quantify the degree of the disorder in fiber orientation, the measurement results were analyzed by Local Moran's *I* and Local Geary's *c*, which are measures of the representative spatial autocorrelation analyses. Quantification by the "area ratio" was optimized by seeking an appropriate threshold level of the measures, correlated closely with tensile strength data.

In the chapter III, finite element method (FEM) is to classify engineering analyses. This method does not acquire the real experimental results, which usually consume time of investment. First of all, fiber waviness was quantified. The composite surface was divided by 1mm x 1mm squares, and the fiber orientation angles to the loading direction were measured on the all squares. Finite element analysis was carried out by recognizing the divided squares as finite elements. Stress-strain relation of the finite element was based on the orthotropic theory, in which the measured angles were assigned to each element. After that the stress results were compared with the experimental tensile strength.

In the chapter IV, the risky areas on specimens were predicted by Tsai-Hill criterion, Tsai-Hill criterion without FEM and Local Geary's *c*. The risky areas of Tsai-Hill criterion and Tsai-Hill criterion without FEM were analyzed the angle patterns around the maximum and minimum Tsai-Hill criterion with maximum and minimum deltas. Furthermore, the relation between the weigh function of Local Geary's c and Tsai-Hill criterion was used to find the risky areas of Tsai-Hill criterion defined by positive delta.

Chapter II Effect of random fiber waviness on tensile strength of a flax-sliver-reinforced composite material

2.1 Introduction

Strong demand for the use of composite materials is increasing today because high strength and stiffness, as well as low density, are needed to reduce energy consumption in aviation and automotive transport industries. The use of artificial fiber-reinforced composite materials, such as glass fiber-reinforced plastics (GFRP) and carbon fiber-reinforced plastics (CFRP), is effective to meet these demands, but disposal difficulties that arise after their use have surfaced as an environmental problem. Therefore, many researchers have strived to develop biodegradable renewable composite materials and various production methods for the materials that will widen their practical availability. Plant based natural fibers, such as flax, hemp, ramie, jute, kenaf, curaua, and bamboo, are expected for use as the composite reinforcement materials, but these are often used as short fibers, as seen in injection-molded products. Long fibers are generally known to exhibit load-bearing potential in a matrix material as compared to short fibers. Before spinning process, plant-based natural fibers are often supplied as long fibers called "slivers."When this form is successfully prepared with resin, slivers can be applied as a semi finished composite material in prepregs. One of the problems in preparing slivers is their fiber waviness, which is fluctuation in the fiber orientation inherent in plant-based natural fibers as well as synthetic fibers. In these papers, however, the fiber waviness was assumed as a deterministic shape such as a sine curve. In order to take the stochastic wavy effect of sliver into account, the fiber orientation fluctuation in curaua-sliver- and flax sliver-reinforced composite through one-dimensional and angles on the composite surface were quantified. The quantified parameter expressing the degree of the fluctuation, called the "area ratio," was correlated with the composite tensile strength. However, the use of autocorrelations was intended to evaluate the

quality of fiber orientation but not to express the degree of local disorder in fiber orientation. In general, stiffness is insensible for structural defects, but strength is sensible. Therefore, the local disorder in fiber orientation is of great interest for quantification through some statistical or stochastic analytical method. It is also expected that the quantified parameter shall play a role as a key indicator during quality inspection for produced prepregs. Thus, the purpose of this study is to examine the effects of the fiber waviness on the tensile strength of a flax-sliver reinforced composite (in-plane tensile modulus). Resin pasted flax slivers were first compression molded, and then fiber orientation angles were measured on the surfaces of the resultant composite laminates. To quantify the degree of the disorder in fiber orientation, the measurement results were analyzed by Local Moran's I and Local Geary's c, which are measures of the representative spatial autocorrelation analyses. Quantification by the "area ratio" was optimized by seeking an appropriate threshold level of the measures, correlated closely with tensile strength data.

2.2 Experimental

2.2.1 Materials

Flax slivers, one of the representative natural fibers, were used as reinforcement as shown in Figure 1. The slivers were supplied from Teikoku Sen-i Co., Ltd., Japan. Biodegradable thermoplastic resin was used as the matrix, which was supplied from Miyoshi Oil and Fat Co., Ltd., Japan (product name: Randy PL-1000). The resin was supplied in a water emulsion containing micro order fine particles of approximately 5.0 μm diameter. The Randy PL-1000 is made from plant-derived biodegradable resins.

Fig.2.1 Flax sliver

Fig.2.2 Resin-pasted sliver

2.2.2 Molding process

First, the fibers on the front side were closed with resin and dried for 24 hours, after that another side (back side) was done with the same process as the front side. At each process the weight was measured for the calculation of fiber content. After finishing preparation of the pre-forms, we cut them into the size 100 mm x 100 mm, and put two pieces into the mold. The mold was set at 150 ^{o}C for 40 min, and then the hydraulic press was set at 3MPa pressure. Subsequently, the temperature was reduced to room temperature at the pressure of 3MPa for 24 hours. The fiber volume fractions V_f of all fabricated composites were calculated using the following equation:

$$V_f = 1 - \frac{W - W_f}{\rho_m V} \qquad (1)$$

where W is the fabricated composite weight, W_f is the flax fiber weight in the composite, V is the fabricated composite volume, and ρ_m is the biodegradable resin density.

Two methods were prepared to fabricate the composites: sheet lamination method (SLM) and the direct method (DM). The latter method is more appropriate for mass production than the former, but the products fabricated by DM include fiber orientation fluctuation. For SLM, the sliver was first combed carefully to form unidirectionally oriented fibers.

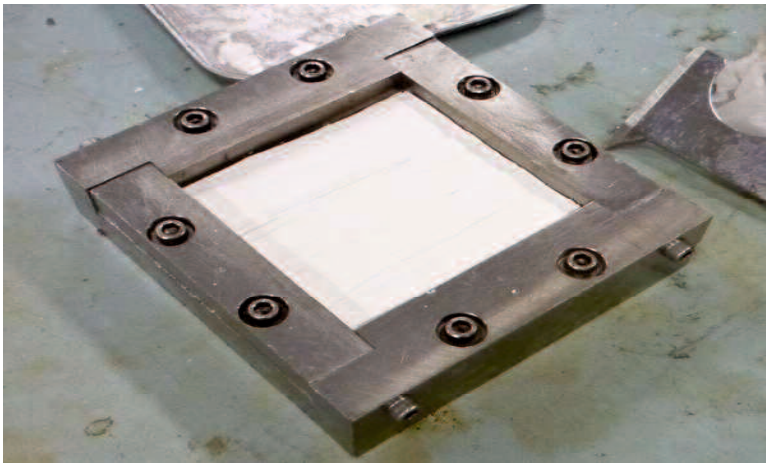

Fig.2.3 Die and perform sheets

Fig.2.4 The combed fibers of sheet lamination method

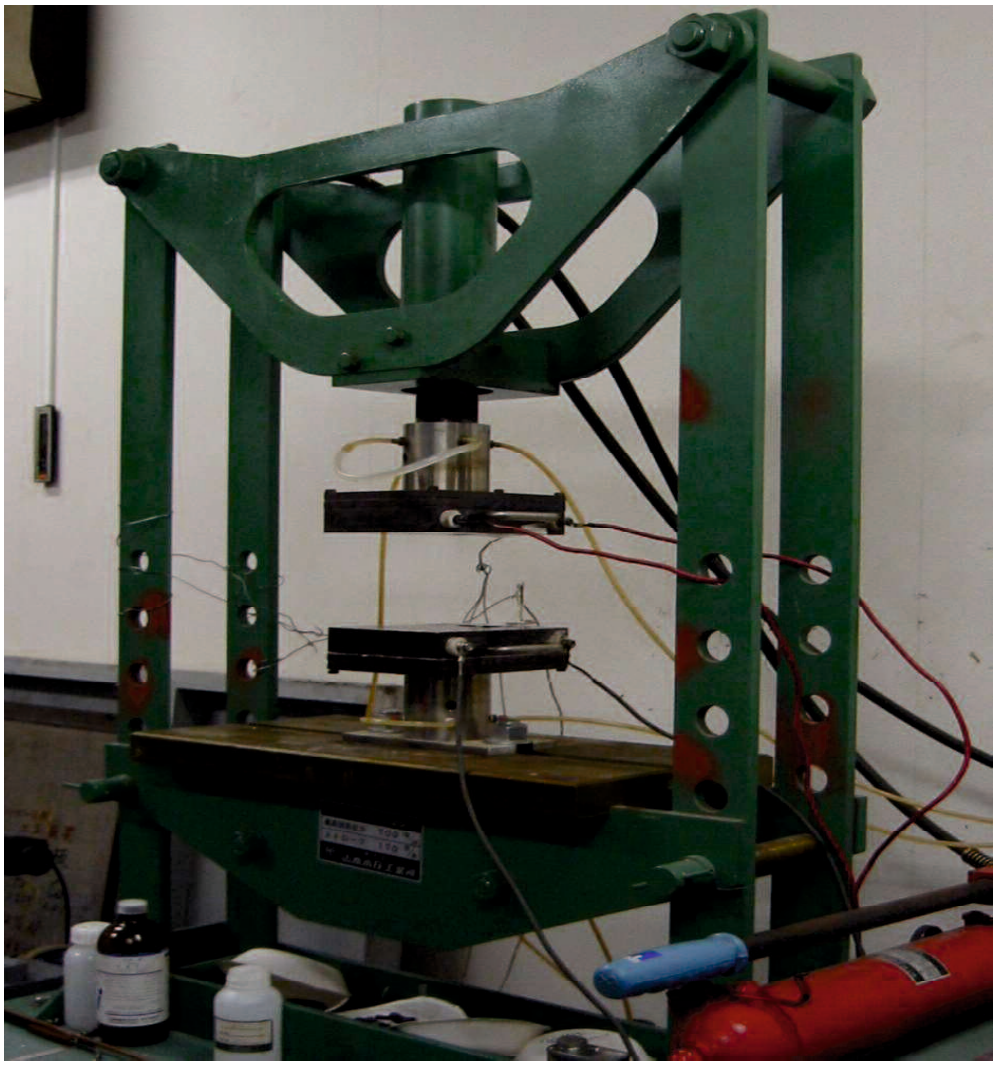

Fig.2.5 Hot-press machine

(Capacity: 20ton, Press only supplied from Yamamoto Suiatu Kogyosho Co., Ltd.)

Fig.2.6 The sheet lamination method (SLM)

Fig.2.7 The direct method (DM)

2.2.3 Angle Measurements

Fiber orientation angles are important data for calculating the stress distribution of composite with fiber waviness. In this process, *x*-axis is the longitudinal direction and *y*-axis is the transverse direction. Specimens were divided into a small size as 1 mm for Δx and Δy which are 50 segments along *x*-axis and 15 segments along *y*-axis, respectively, so the total number of segments is 750 for each side (Fig.3). The image analysis software (Asahi Kasei Corp) was used for angle measurement of each segment.

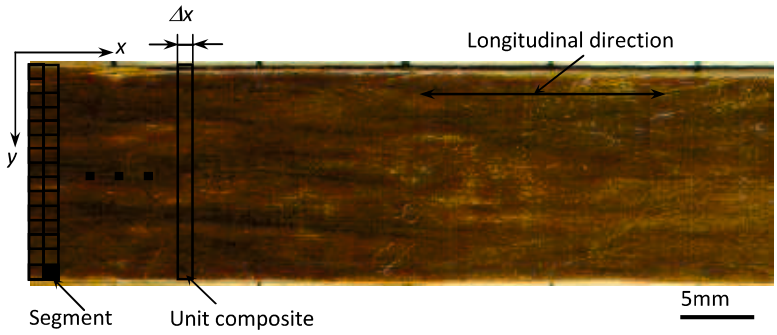

(a) Division into segment

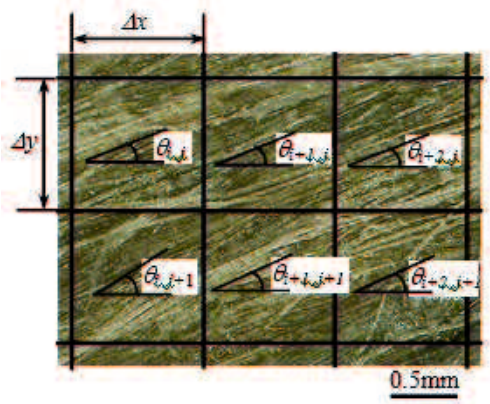

(b) Angle θ in a segment (Δx=Δy=1 mm)

Fig.2.8 Measurement of fiber orientation angles on flax sliver-reinforced composites.

2.2.4 Tensile tests

Tensile specimens were cut to 15mm width from DM and SLM composite laminates of 100mm× 100mm square, and then aluminum plates (15mm × 15 mm) were attached with epoxy adhesive to both ends of all composite specimens for tensile testing. To prevent stress concentration near aluminum plates during tensile testing, their edges were shaved to 45°. A strain gage was attached on the center of specimens to measure uniaxial strain. Tensile tests were carried out using an Instron-type testing machine (Autograph IS-500; Shimadzu Corp.) with cross-head speed of 1 mm/min. The strain rate is 0.02/min and load is 50N.

Fig.2.9 Instron type tension and compression machine

The specimens were preformed as length and width is 100mm x 15mm, thickness is 0.4 to 0.8mm and gage length is 50mm.

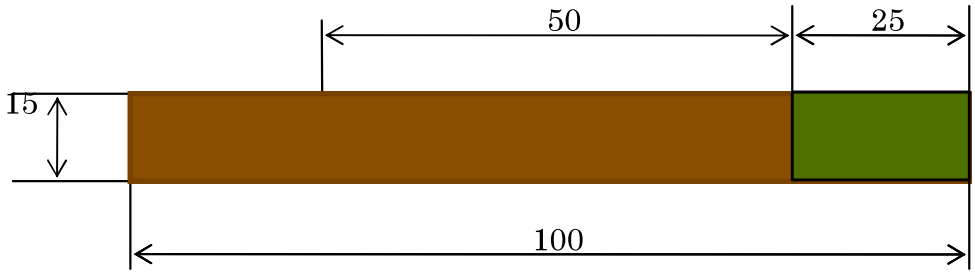

Fig.2.10 The specimen size

Fig.2.11 the position of strain gage on specimens

2.2.5 Spatial Autocorrelation Analysis

Spatial autocorrelation is a method to analyze point patterns. The point patterns are differentiated as random pattern, uniform pattern and patch pattern.

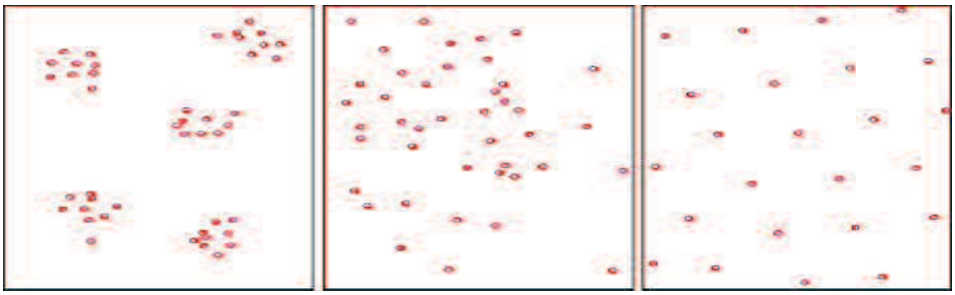

(a) patch pattern (b) random pattern (c) uniform pattern

Fig.2.12 Differentiated point patterns

2.2.5.1 Local Moran's *I*

Local Moran's *I* was created by Moran. It is a typical tool of spatial autocorrelation to analyze data because it is based on a deviation from the average. The equation of Local Moran's *I* is shown as:

$$I_i(d) = \frac{(\theta_i - \overline{\theta})}{\frac{1}{n}\sum_{i=1}^{n}(\theta_i - \overline{\theta})^2} \sum_{\substack{j=1 \\ j \neq i}}^{n} w_{ij}(d)\left(\theta_j - \overline{\theta}\right) \qquad (2)$$

Where, $w_{ij}(d)$ is the weight function of the pair samples in distance class d at equation (3), given as:

$$w_{ij}(d) = \left\{(x_i - x_j)^2 + (y_i - y_j)^2\right\}^{-\frac{1}{2}} \qquad (3)$$

where x_i is i-th position of the x-axis, and the range is 1–50 mm. Also, y_i is the i-th position of the y-axis, and the range is 1–15 mm. θ_i and θ_j are the angle data at the i-th and j-th positions, respectively. Hereinafter, Local Moran's *I* is denoted as LM-*I*. LM-*I* varies between -1 to +1. If LM-*I* approaches +1, then the angle at this location is more largely far from the average, but similar to the neighbor's angles in their deviation from the average. On the other hand, if LM-*I* tends to approach -1, then the angle at this location is also higher or lower than the average. But, the sign is different from the neighbor angles. When LM-*I* tends to approach 0, the angle at this location is similar to the average. Theoretically, when LM-*I* is either much higher or lower than 0, then the fiber orientation angle is significantly different from the average. Consequently, such LM-*I* points, if gathered locally, could form a large disordered area in fiber orientation.

2.2.5.2 Local Geary's *c*

Local Geary's *c* is another typical spatial autocorrelation, which avoids the effect of average data by using a deviation around *i*-th position. The equation of Local Geary's *c* is shown as:

$$C_i(d) = \frac{1}{\frac{1}{n}\sum_{i=1}^{n}(\theta_i - \bar{\theta})^2} \sum_{\substack{j=1 \\ j \neq i}}^{n} w_{ij}(d)(\theta_i - \theta_j)^2 \qquad (4)$$

Local Geary's *c* is hereinafter denoted as LG-*c*. LG-*c* varies between 0 and 1. When LG-*c* tends to approach 0, the angle at this location is similar to the neighbor angles. In contrast, when LG-*c* tends to approach 1, the angle at this location differs from the sign of neighbor angles or much higher than the neighbor's angles in absolute value. Consequently, such points can be disordered parts in fiber orientation.

2.3 Results and discussions

2.3.1 Tensile Properties and Fiber Orientation Angle

This study aims to analyze the effect of fiber waviness on the tensile strength of sliver-based natural fiber composites. The test results are shown in Table 2.1 The tensile strength of the direct method (DM), which consists of plenty fiber waviness, is lower than the sheet laminate method (SLM) for all specimens. Fiber waviness was quantified by the fiber orientation angles. According to the contour maps of fiber orientation angle distribution in fig. 2.13, they have a wide range of positive twenty degrees to negative twenty degrees.

Table 2.1 Fiber orientation angles and mechanical properties of flax sliver-reinforced composites.

Production method	Specimens						Tensile strength (MPa)	Young's modulus (GPa)
	Sample No.	Fiber volume fraction	Side A (lower angle)		Side B (higher angle)			
			Avg. angle (°)	S.D. of angles (°)	Avg. angle (°)	S.D. of angles (°)		
SLM	-	0.71	0	-	0	-	238	40.5
DM	<1>	0.55	1.99	3.54	3.30	4.28	132	22.7
	<2>	0.55	2.62	5.22	4.19	4.03	224	26.7
	<3>	0.55	5.14	4.06	5.55	3.18	158	29.6
	<4>	0.55	3.05	3.22	8.76	4.18	211	27.6
	<5>	0.65	1.74	3.73	2.85	2.66	158	23.3
	<6>	0.65	2.10	2.62	3.07	3.48	203	26.4
	<7>	0.65	1.61	2.33	2.20	2.32	153	27.5
	<8>	0.65	2.08	3.47	3.76	2.95	170	28.0
	<9>	0.65	1.45	3.72	5.26	4.77	173	26.8
	<10>	0.65	0.76	3.50	4.55	3.90	168	28.8
	Avg.	0.61	2.35	3.50	4.35	3.60	175	26.8

The number of SLM specimens was seven. Avg.: Average, S.D.: Standard deviation.

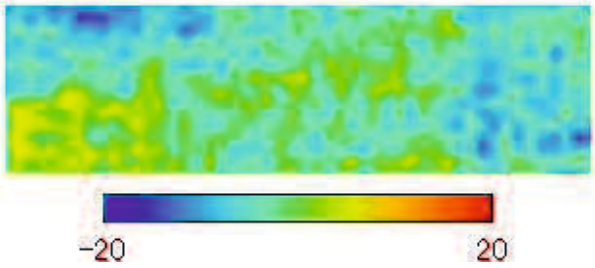

(a) Specimen no.1A

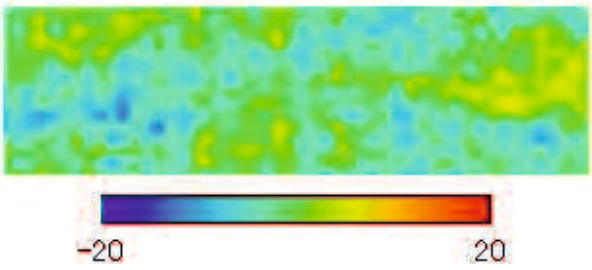

(b) Specimen no.1B

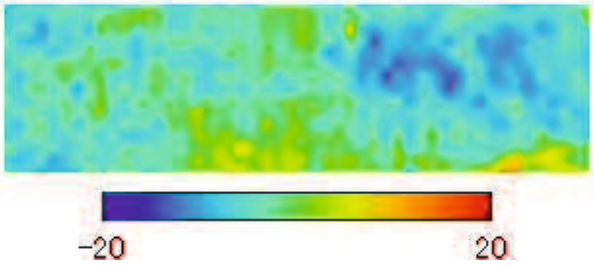

(c) Specimen no.2A

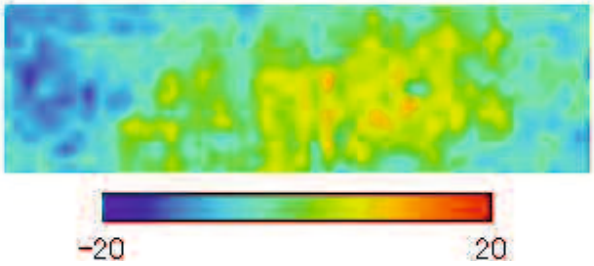

(d) Specimen no.2B

Fig. 2.13 Contour map of fiber orientation angle distribution

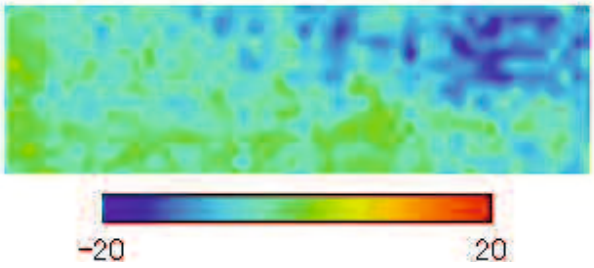

(e) Specimen no.3A

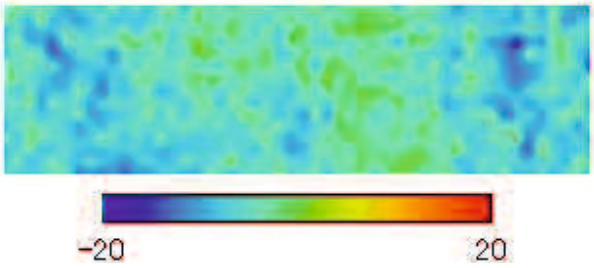

(f) Specimen no.3B

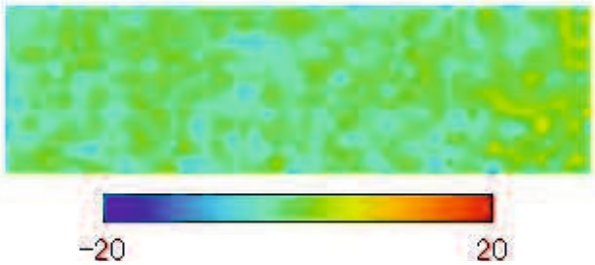

(g) Specimen no.7A

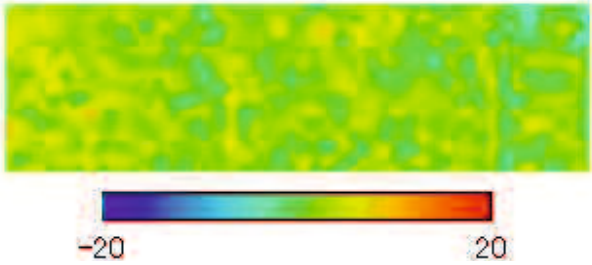

(h) Specimen no.7B

Fig. 2.13 Contour map of fiber orientation angle distribution

2.3.2 Spatial Analysis's results

Spatial analysis is used for defining the effect location of random fiber waviness on tensile strength. As first method, Local Moran's *I*, I coefficient varies between -1 to +1. Regarding, the inclination of I coefficient to approach +1, the value at this location is similar the neighbor location in their deviation from the average. On the other hand, I coefficient trends to approach -1, thus the value at this location is different from the average in higher or lower. Additionally, the sign is different from the neighbor locations. In the case, I coefficient trends to approach 0, the value at this location is similar to the average. Theoretically, the coefficient, which is either higher or lower than 0, means the fluctuation in fiber orientation varied significantly from the average angle. As a result, it could reduce the tensile properties. The results of Local Moran's *I* are shown in fig.2.14.

Regarding the coefficient of Local Geary's *c,* it varies between 0 and 1. The *C* coefficient tends to approach 0, thus the value at this location is similar to the neighbor location. In contrast, the *C* coefficient trends to approach 1, thus value at this location is different from the sign of neighbor locations. In the case, the coefficient trends to 0, thus the value at this location is similar to the neighbor locations. The results of Local Geary's *c* are shown in fig.2.15.

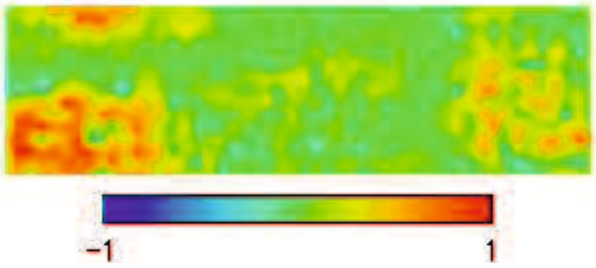

(a) Specimen no.1A

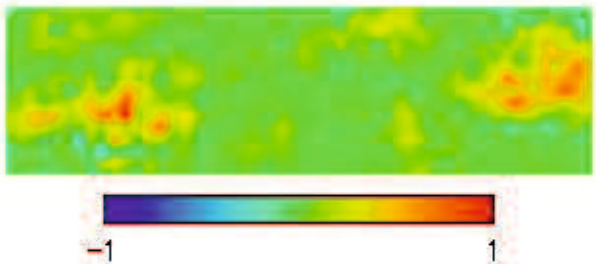

(b) Specimen no.1B

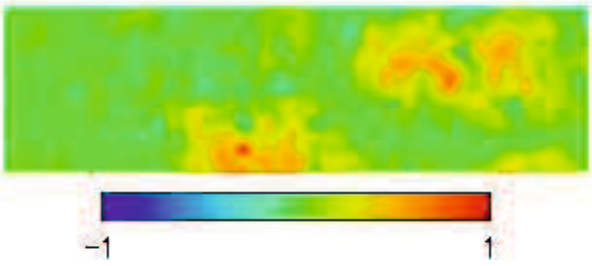

(c) Specimen no.2A

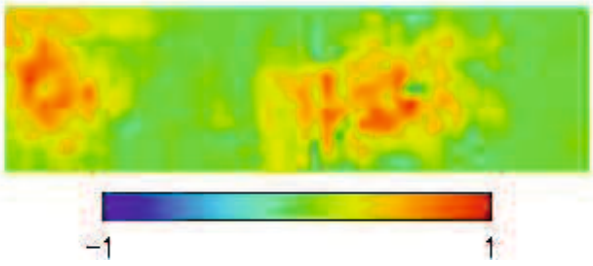

(d) Specimen no.2B

Fig. 2.14 Contour maps of Local Moran's *I* distribution

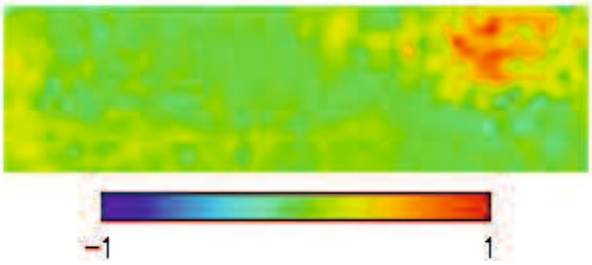

(e) Specimen no.3A

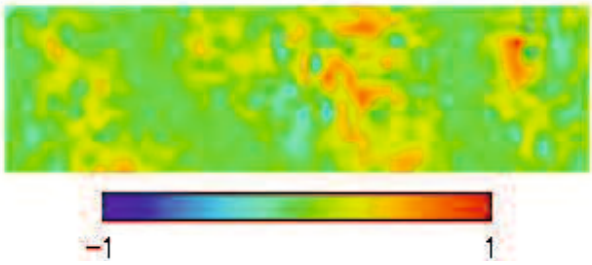

(f) Specimen no.3B

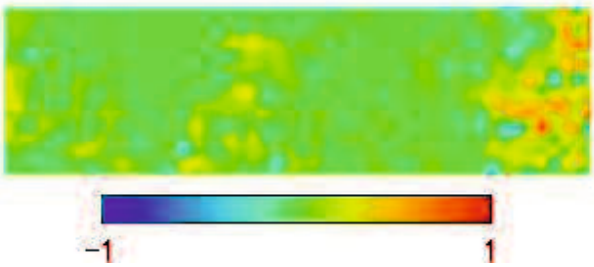

(g) Specimen no.7A

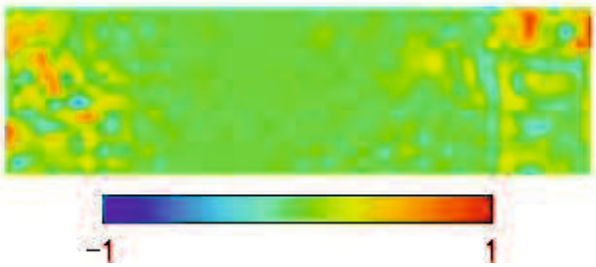

(h) Specimen no.7B

Fig. 2.14 Contour maps of Local Moran's *I* distribution

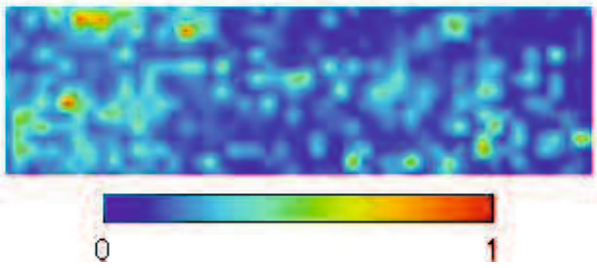

(a) Specimen no.1A

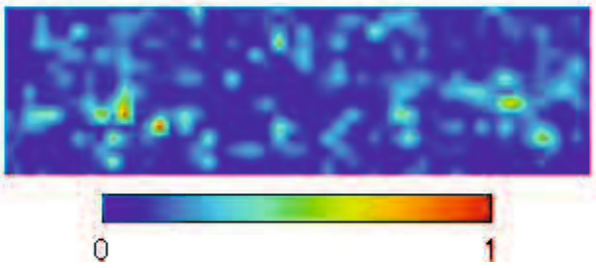

(b) Specimen no.1B

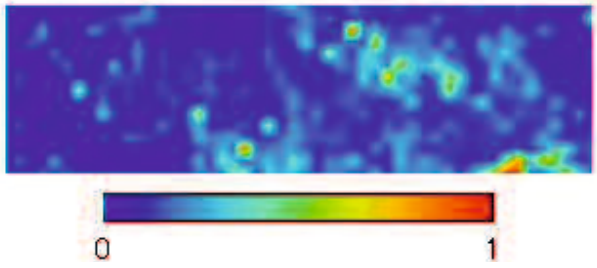

(c) Specimen no.2A

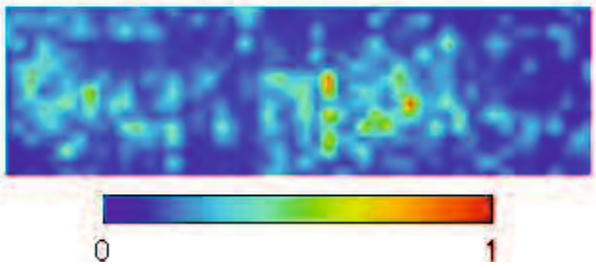

(d) Specimen no.2B

Fig. 2.15 Contour maps of Local Geary's *c*

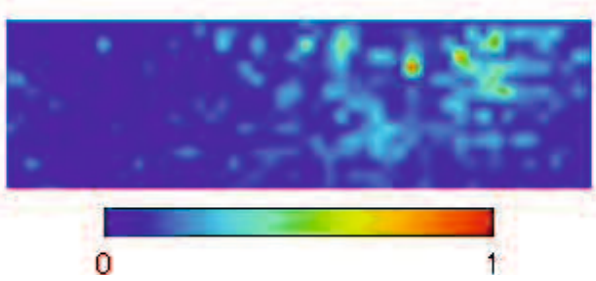

(e) Specimen no.3A

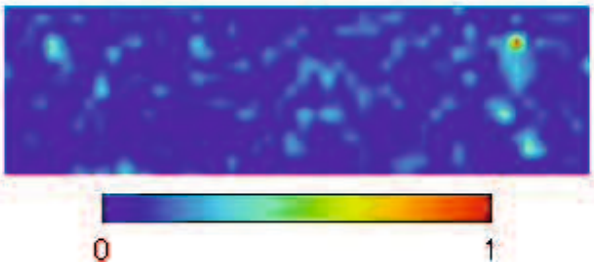

(f) Specimen no.3B

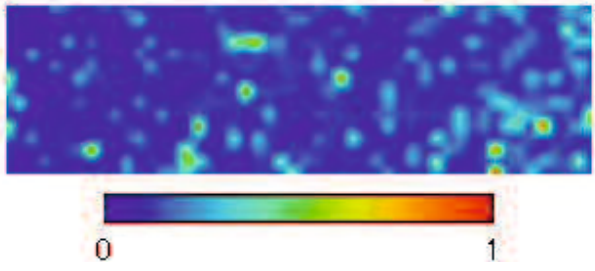

(g) Specimen no.7A

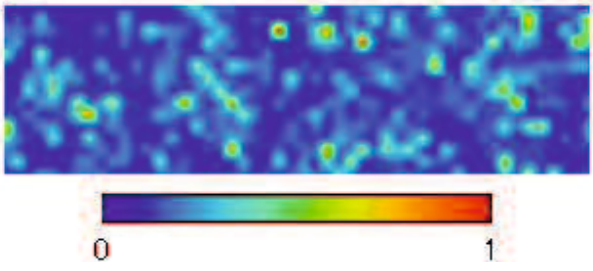

(h) Specimen no.7B

Fig. 2.15 Contour maps of Local Geary's *c*

2.3.3 Area ratio

In this research, we tried to quantify the 'threshold levels' of spatial analyses by using the concept of 'area ratio'. If the area ratios are well correlated with tensile strength data, the strength could be estimated from the fiber orientation angle distribution measured in advance. In this quantification, we used two imaging programs; first 'Graph R221' was used for plotting a contour map of the above three methods, and next 'Azo R235' used to calculate area ratio.

When we choose temporarily threshold levels higher than 0.6 or less than -0.1, the black areas of LM-*I* were obtained, as shown in Fig. 2.16(a) to Fig. 2.16(d). The area ratios of specimens were 10.267% (positive side =5.067% and negative side =5.2%), 4.267% (positive side =1.467% and negative side =2.8%), 6.267% (positive side =0.8% and negative side =5.467%), and 11.6% (positive side =2% and negative side =9.6%) for the specimen number 1A, 1B, 7A and 7B respectively. The range of negative values is designated more widely than that of positive value, because the segments with negative LM-*I* values are not so major, but have a possibility of causing premature damage in shear. Thus, wide range negative values and relatively high positive values are corresponding to risky areas. In Fig 2.17(a) to Fig. 2.17(d), the black areas of LG-*c* are higher than 0.35 were selected. The area ratios of specimens were 12.80%, 4.533%, 5.333% and 9.467% for specimen number 1A, 1B, 7A and 7B respectively. As is easily known, when the threshold levels of TH, LM-*I* and LG-*c* are changed, the area ratios accordingly change. We consider, if appropriate threshold levels are given, there is an optimal area ratio at each specimen which is well correlated with tensile strength. This is because the ratio of segments suffering damage during tensile loading should be related closely with the area ratio. In the next section, thus, the relation between area ratio and tensile strength is investigated.

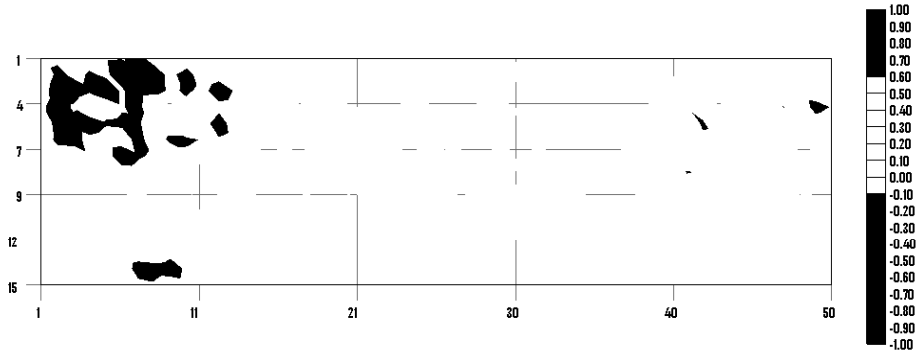

(a) Specimen no.1A

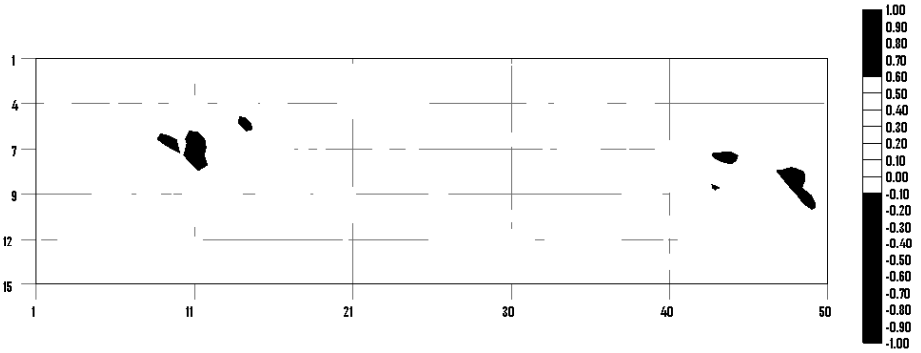

(b) Specimen no.1B

Figure 2.16 Binary images of Local Moran's *I* distribution

(threshold levels: positive LM-I = 0.60 and negative LM-I = –0.10)

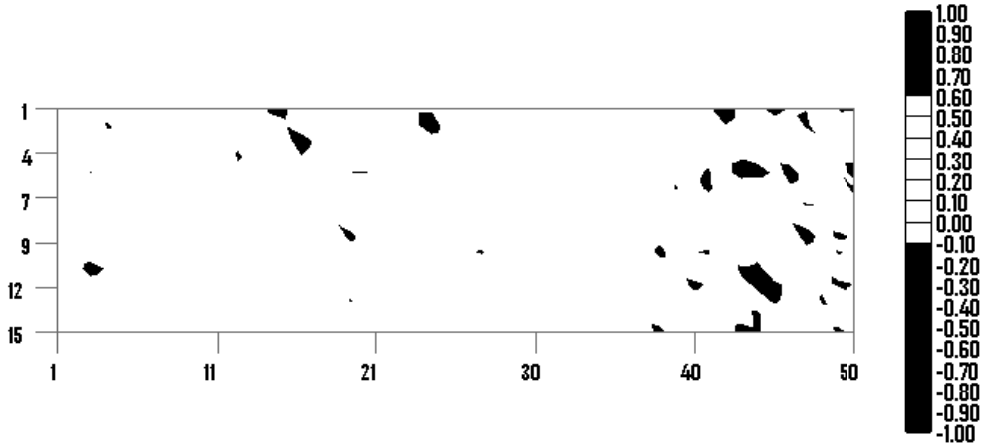

(c) Specimen no.7A

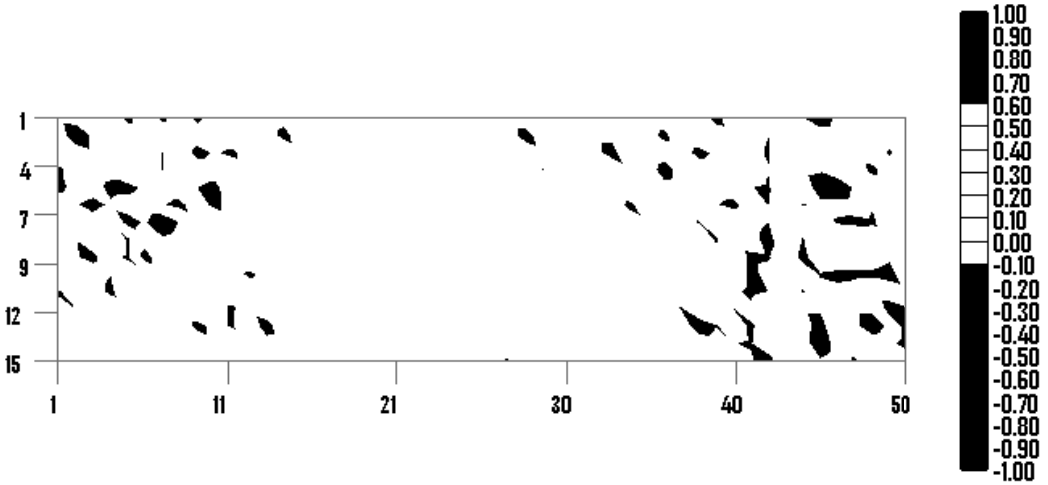

(d) Specimen no.7B

Fig. 2.16 Binary images of Local Moran's I distribution

(threshold levels: positive LM-I = 0.60 and negative LM-I = –0.10)

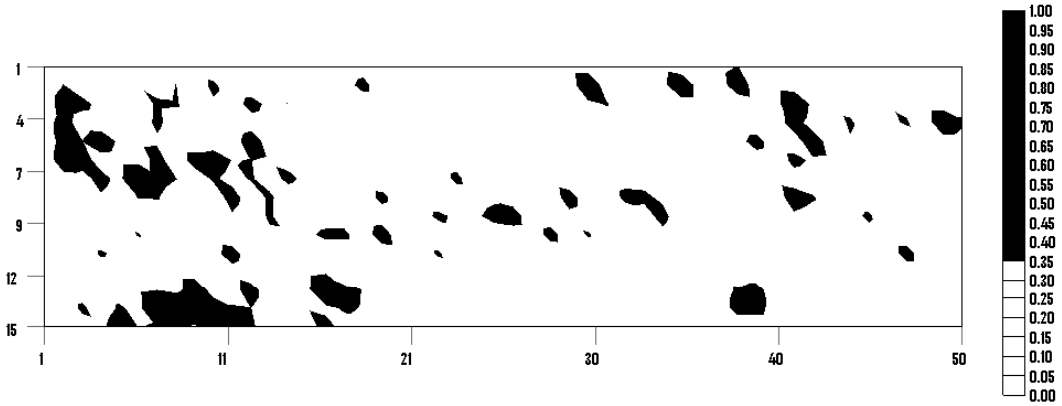

(a) Specimen no.1A

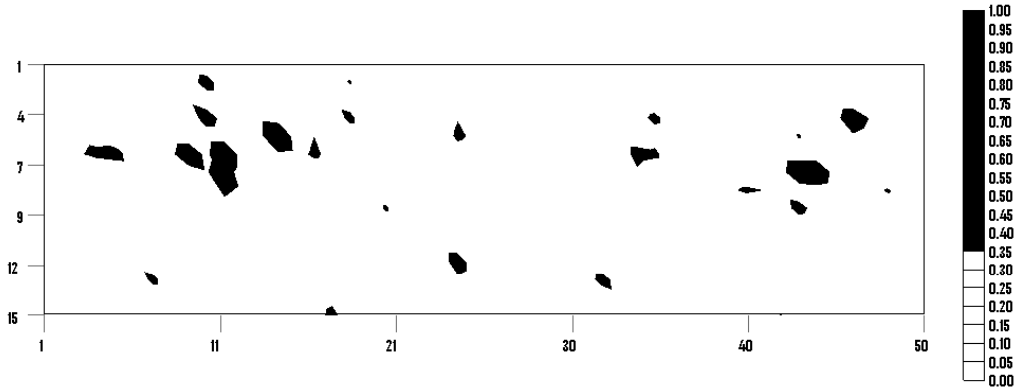

(b) Specimen no.1B

Fig. 2.17 Binary images of Local Geary's c distribution (threshold level: LG-c = 0.35)

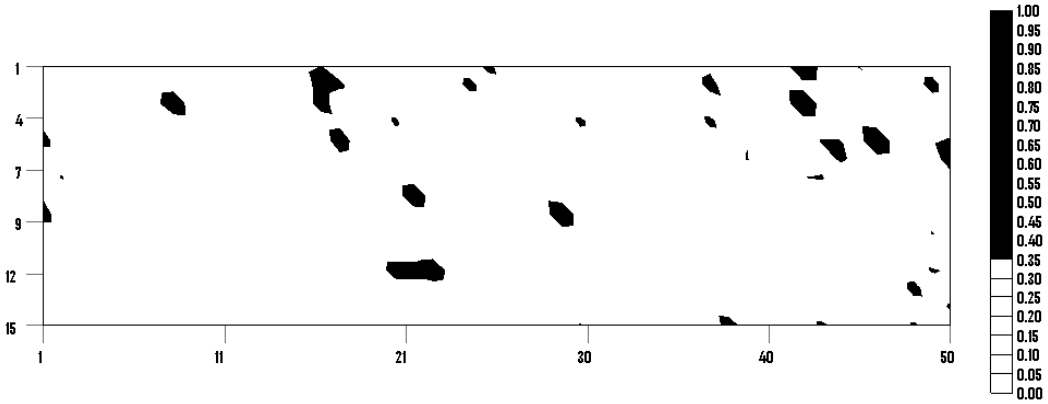

(c) Specimen no.7A

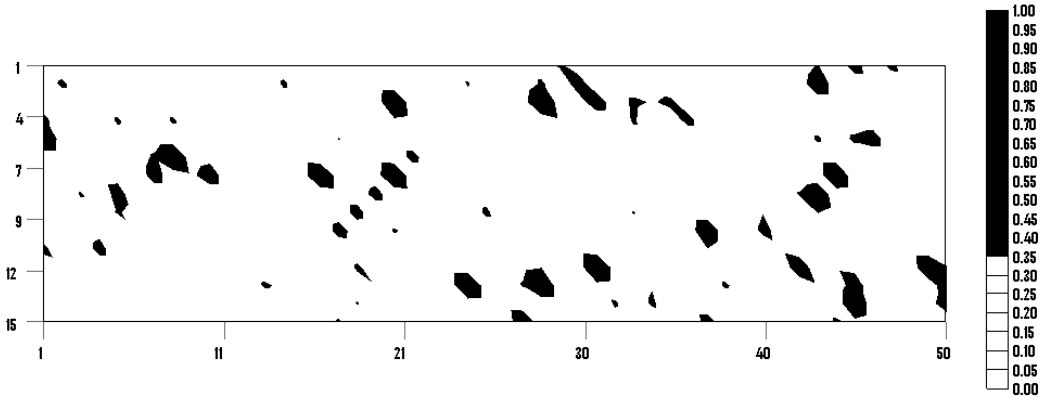

(d) Specimen no.7B

Fig. 2.17 Binary images of Local Geary's *c* distribution (threshold level: LG-*c* = 0.35)

2.3.4 Relation between Area Ratio and Tensile Strength

To investigate the correlation between the area ratio and tensile strength, normalized tensile strength data were plotted as a function of area ratio, as shown in Figures 2.18 and 2.19, where each tensile strength value was normalized at the same fiber volume fraction. That is to say, the tensile strengths were normalized by dividing the measured strength by the fiber volume fraction V_f and then multiplying it by 0.72, corresponding to V_f of SLM specimen. In Figures 2.18 and 2.19, they appear that the normalized strength is correlated with the area ratio. The correlation coefficients of Local Moran's I were calculated as -0.44 and −0.65 when setting threshold levels at LM-I > 0.6 or LM-I < -0.1 in Fig.2.18 (a) and LM-I > 0.8 or LM-I < -0.1 in Figures 2.18 (b).The value of −0.65 is not so strong but presents an intermediate strong correlation. This means that if many segments in a specimen are distributed with LM-I values higher or lower than the above threshold levels, its tensile strength tends to be lowered. It also means that a rough value of tensile strength can be estimated through the least-squares regression line between area ratio and tensile strength.

In contrast, the correlation coefficients of Local Geary's c between the area ratio and tensile strength were 0.18 and 0.29, when setting threshold levels at 0.2 and 0.5 respectively. The value of 0.29 signifies weak correlation. This result implies that 0.29 is not appropriate as a threshold level or that Local Geary's c does not match correlation with tensile strength.

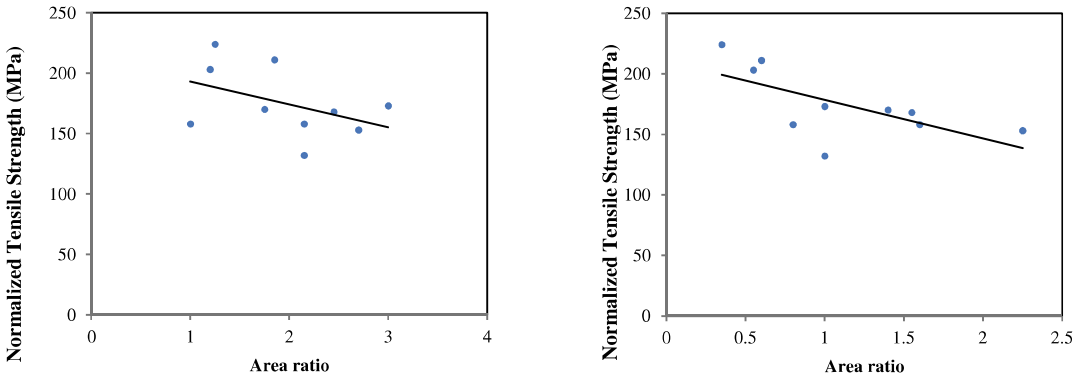

(a) Threshold levels: LM-*I* > 0.6 or LM-*I* <-0.1 (b) Threshold levels: LM-*I* > 0.8 or LM-*I* < -0.1

Fig. 2.18 LM-*I* area ratio dependence on normal tensile strength

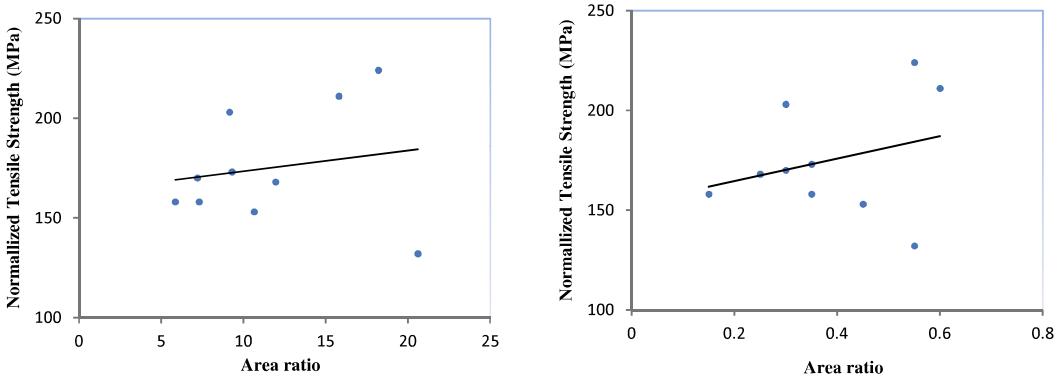

(a) Threshold levels: LG-*c* > 0.2 (b) Threshold levels: LG-*c* > 0.5

Fig. 2.19 LG-*c* area ratio dependence on normal tensile strength

The results are shown in Figs. 2.20 and 2.21. It is confirmed in Fig. 2.20 that the optimal threshold levels of LM-*I* are 0.69 at the positive level and -0.10 at the negative level, and that of LG-*c* is 0.36. At the former optimal threshold levels, the correlation coefficient between area ratio and tensile strength was -0.832. On the other hand, the highest correlation coefficient in Fig. 2.21 was only -0.14 even at the optimal threshold level. The value of -0.832 means, there is a strong negative correlation between area ratio and tensile strength. In other words, tensile strength can be estimated to some degree through the least-squares regression line when setting the optimal threshold levels of LM-*I*. It is also expected that the present procedure is applied as an effective screening method extracting low quality prepregs at quality inspection.

Fig.2.20 Correlation coefficients between LM-I area ratio and normalized tensile strength vs. negative threshold level

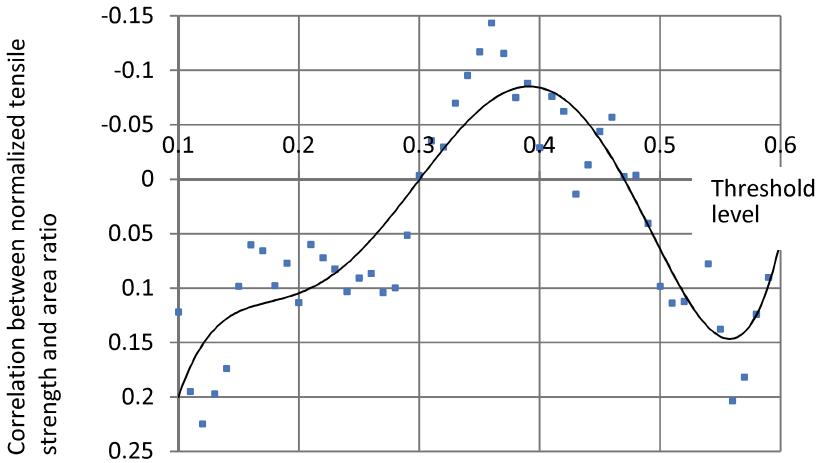

Fig.2.21 Correlation coefficients between LG-c area ratio and normalized tensile strength vs. threshold level

2.4 Conclusions

This study clarified the effect of random fiber waviness on tensile strength of a flax-sliver-reinforced biodegradable resin matrix composite material. The fiber waviness was quantified using Local Moran's *I* and Local Geary's *c*, both of which were able to express the degree of disorder in fiber orientation. The results show that Local Moran's *I* is correlated well with tensile strength of the composite specimens when appropriate threshold levels are selected. On the other hand, Local Geary's *c* is not well correlated with tensile strength. Normally, finite element analysis is a well-known method for finding mechanical behavior of composite materials, such as stress and strain distributions. Furthermore, finite element analysis is often extended to

the fracture process simulation to predict strength properties. However, finite element method needs to use several math models to find the solution that take time and the advanced knowledge for understanding. On the other hand, this study using the spatial autocorrelation analysis has less equation and does not take a long time for developing the program code. Thus, we conclude that the method proposed in this study is an effective tool of predicting roughly the tensile strength of natural-fiber-sliver-based composite materials.

Chapter III Finite element analysis of a natural fiber sliver- reinforced composite

3.1 Introduction

Recently, fibrous composite materials such as GFRP (glass fiber-reinforced plastics) and CFRP (carbon fibber-reinforced plastics) are effectively applied for the high demand in industrial use because their advantages are light weight, high strength and corrosion resistance. However, the disposal problem after use of these materials has also surfaced as an environmental problem. To solve this problem, many researchers have tried to use plant-based natural fibers instead of artificial fibers. However, a problem of using natural fiber is fiber waviness that affects the tensile properties. Fiber waviness is the fluctuation in fiber orientation, inherent in sliver morphology of plant-based natural fibers. Therefore, the finite element method (FEM) was able to clarify the stress on the specimens in this study.

Finite element method (FEM) is a well-known method, applicable to classify engineering analyses. This method does not acquire the real experimental results, which usually consume time of investment. First of all, fiber waviness was quantified. The composite surface was divided by 1mm x 1mm squares, and the fiber orientation angles to the loading direction were measured on the all squares. Finite element analysis was carried out by recognizing the divided squares as finite elements. Stress-strain relation of the finite element was based on the orthotropic theory, in which the measured angles were assigned to each element. After that the stress results were compared with the experimental tensile strength.

3.2. Finite element analysis

In this study, three-dimensional finite element method was used for calculating stress distribution of the sliver-based green composite. The type of finite element applied was the eight-node hexahedral isoparametric element. Gauss–Legendre algorithm was used for calculating the function, where the number of gauss points (*NG*) is 2. This curve function is 3rd order (cubic). Completely-aligned sliver is a unidirectional fibrous material. The composite reinforced with this material behaves orthotropically, so that its stress–strain relation should be given as equation 1, and the condition of an experiment is one plane of material property symmetry.

$$\begin{Bmatrix} \sigma_x \\ \sigma_y \\ \sigma_z \\ \tau_{yz} \\ \tau_{zx} \\ \tau_{xy} \end{Bmatrix} = [T_{ij}]^{-1} \begin{bmatrix} C_{11} & C_{12} & C_{13} & 0 & 0 & 0 \\ C_{12} & C_{22} & C_{23} & 0 & 0 & 0 \\ C_{13} & C_{23} & C_{33} & 0 & 0 & 0 \\ 0 & 0 & 0 & C_{44} & 0 & 0 \\ 0 & 0 & 0 & 0 & C_{55} & 0 \\ 0 & 0 & 0 & 0 & 0 & C_{66} \end{bmatrix} [T_{ij}] \begin{Bmatrix} \varepsilon_x \\ \varepsilon_y \\ \varepsilon_z \\ \gamma_{yz} \\ \gamma_{zx} \\ \gamma_{xy} \end{Bmatrix} \quad (1)$$

Where, $[T_{ij}]$ is the coordinate transform matrix. The stiffness matrix components, c_{ij} for an orthotropic material in terms of the engineering constants is shown as:

$$C_{11} = \frac{1 - v_{23}v_{32}}{E_2E_3\Delta}, C_{22} = \frac{1 - v_{13}v_{31}}{E_1E_3\Delta}, C_{12} = \frac{v_{21} + v_{31}v_{23}}{E_2E_3\Delta} = \frac{v_{12} + v_{32}v_{13}}{E_1E_3\Delta},$$

$$C_{23} = \frac{v_{32} + v_{12}v_{31}}{E_1E_3\Delta} = \frac{v_{23} + v_{21}v_{13}}{E_1E_2\Delta}, C_{13} = \frac{v_{31} + v_{21}v_{32}}{E_2E_3\Delta} = \frac{v_{13} + v_{12}v_{23}}{E_1E_2\Delta},$$

$$C_{33} = \frac{1 - v_{12}v_{21}}{E_1E_2\Delta}, C_{44} = G_{23}, C_{55} = G_{31}, C_{66} = G_{12}$$

$$\Delta = \frac{1 - v_{12}v_{21} - v_{23}v_{32} - v_{31}v_{13} - 2v_{21}v_{32}v_{13}}{E_1E_2E_3}$$

Elastic constants used here are as follows: when we set the fiber volume faction (V_f) as 0.70, E_1 and E_3= 3210 MPa, E_2= 39500 MPa, v_{21} and v_{13} =0.401, v_{12} and v_{32} =v_{21}*E_1/ E_2. These original constants were obtained experimentally, and estimated to the constant values at V_f =0.7 shown in the above through the rule of mixture and Reuss rule. G_{12} and G_{23}=1610 MPa. These shear moduli was assumed as $E_1/2$ through the reference [14]. G_{31} was also assumed as being $G_{12}/2$ from the reference [15].

The measured fiber orientation angle was substituted into θ. When *Y*-axis is placed as the longitudinal direction, a fiber alignment has an angle θ to *Y*-axis on *X*-*Y* plane. In this study, another angle on *Y*-*Z* plane is not taken into consideration, because the fibers in the prepared pre-forms are in-plane array. Then, the stress components calculated from the present FE analysis are changed through equation (2) to the stresses along the fiber-axis coordinate 1-2-3.

$$\begin{bmatrix} \sigma_1 \\ \sigma_2 \\ \sigma_3 \\ \tau_{23} \\ \tau_{31} \\ \tau_{12} \end{bmatrix} = \begin{bmatrix} m^2 & n^2 & 0 & 0 & 0 & 2mn \\ n^2 & m^2 & 0 & 0 & 0 & -2mn \\ 0 & 0 & 1 & 0 & 0 & 0 \\ 0 & 0 & 0 & m & -n & 0 \\ 0 & 0 & 0 & n & m & 0 \\ -mn & mn & 0 & 0 & 0 & m^2 - n^2 \end{bmatrix} \begin{bmatrix} \sigma_x \\ \sigma_y \\ \sigma_z \\ \tau_{yz} \\ \tau_{zx} \\ \tau_{xy} \end{bmatrix}, \qquad (2)$$

Where, m=cosθ, n=sinθ. The boundary condition is a forced displacement, which is applied at one end of the finite element mesh along *Y*-axis, as shown in Fig.3.1. Another end is fixed along *Y*-axis.

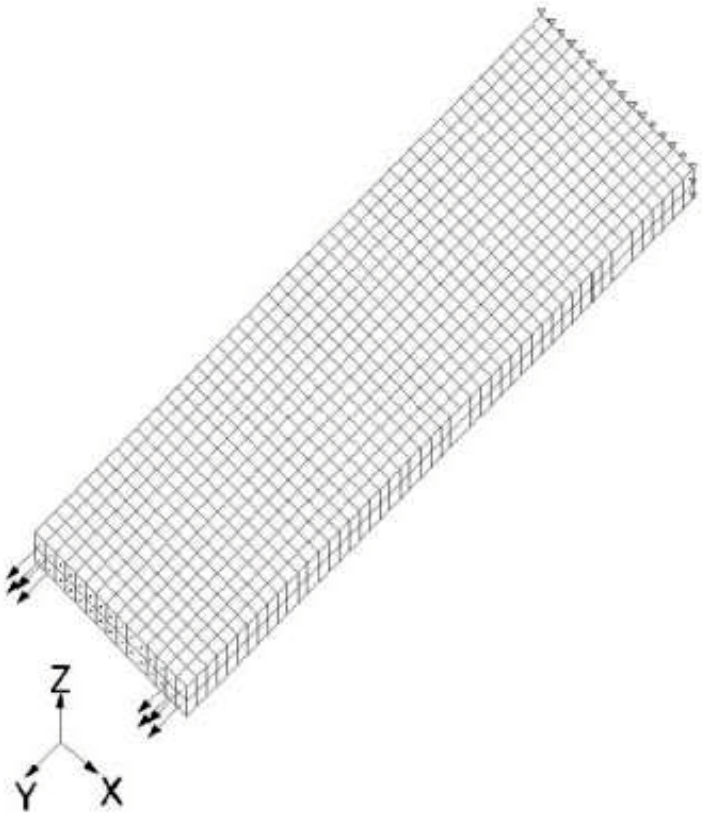

Fig.3.1 Three-dimensional representation of finite element mesh

3.3 Results and discussions

Regarding the results from the finite element method, the tensile stresses in the direction 1, 2 and 3 and shear stresses in 23, 31 and 12 were calculated and shown the failure criteria in the next chapter. The contour maps of the tensile stress and shear stress distribution were shown in fig. 3.2 to fig.3.8.

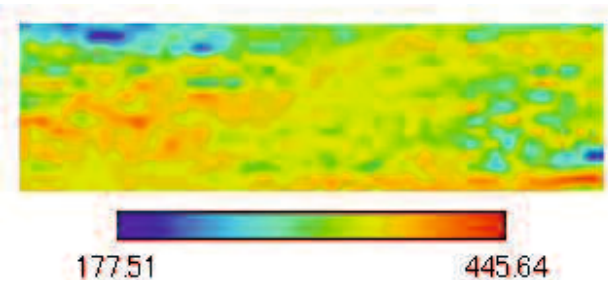

(a) Specimen no.1A

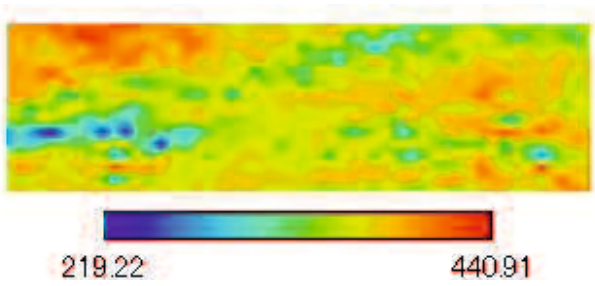

(b) Specimen no.1B

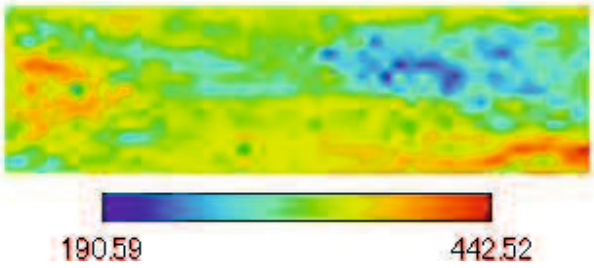

(c) Specimen no.2A

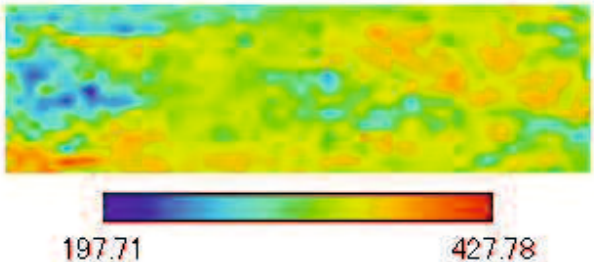

(d) Specimen no.2B

Fig. 3.2 Contour maps of stress distribution in 2-direction

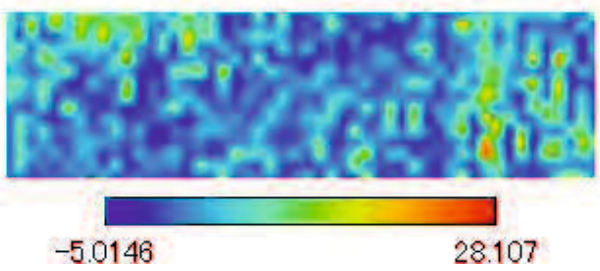

(a) Specimen no.1A

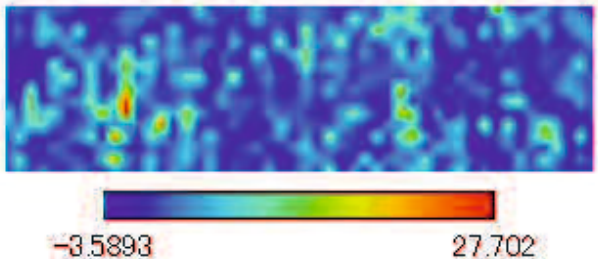

(b) Specimen no.1B

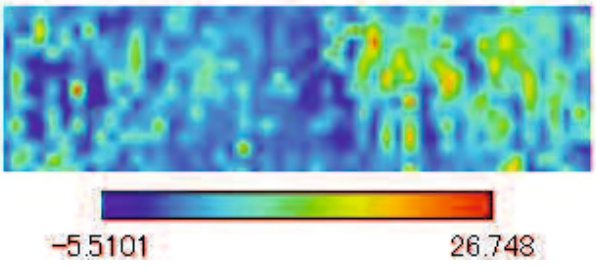

(c) Specimen no.2A

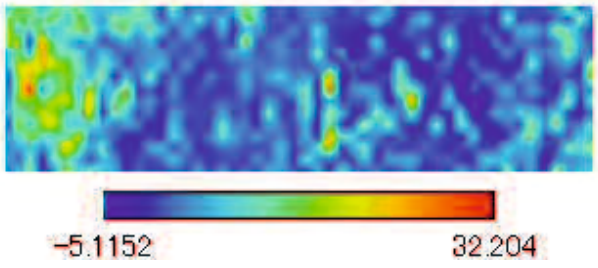

(d) Specimen no.2B

Fig. 3.3 Contour maps of stress distribution in 1-direction

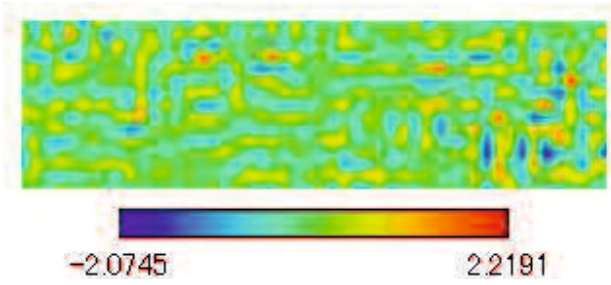

(a) Specimen no.1A

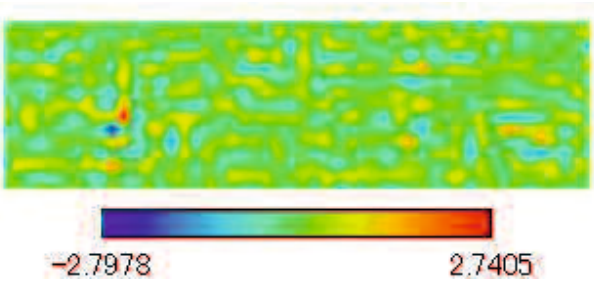

(b) Specimen no.1B

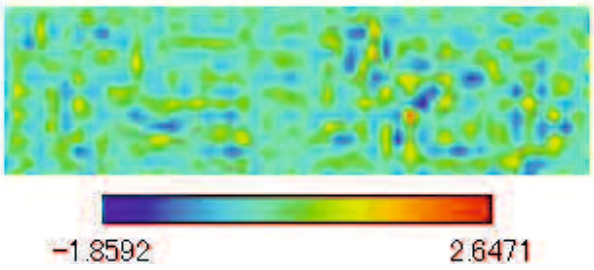

(c) Specimen no.2A

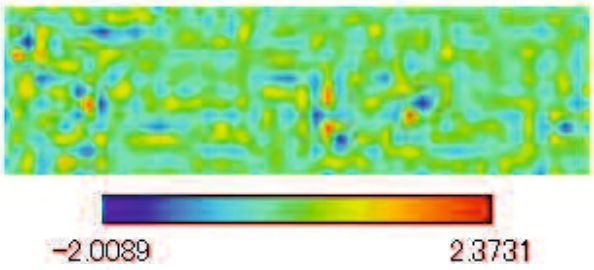

(d) Specimen no.2B

Fig. 3.4 Contour maps of stress distribution in 3-direction

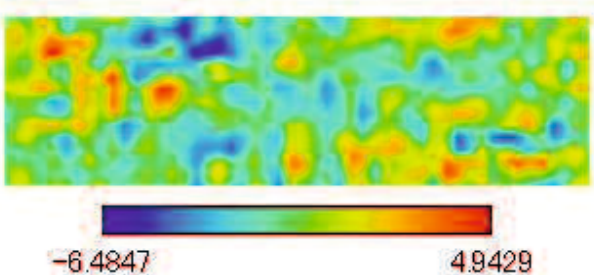

(a) Specimen no.1A

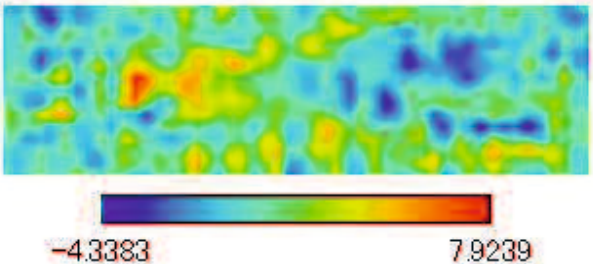

(b) Specimen no.1B

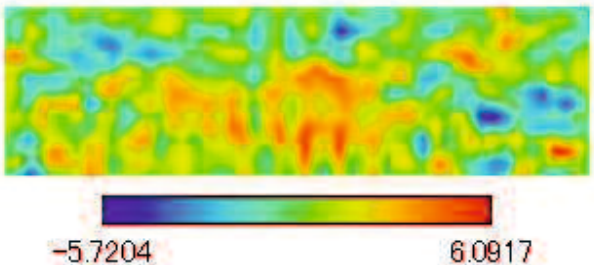

(c) Specimen no.2A

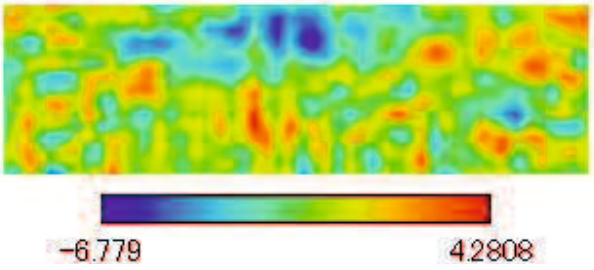

(d) Specimen no.2B

Fig. 3.5 Contour maps of stress distribution in 2-3-direction

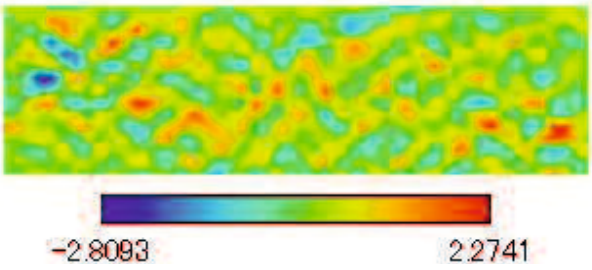

(a) Specimen no.1A

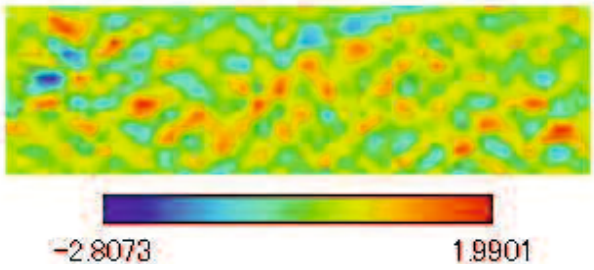

(b) Specimen no.1B

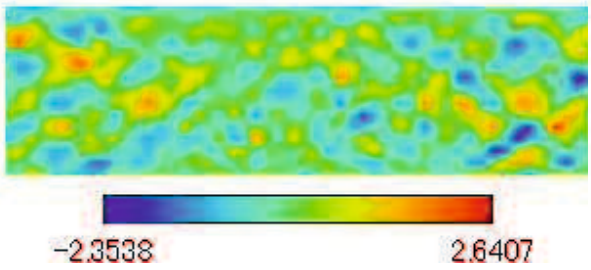

(c) Specimen no.2A

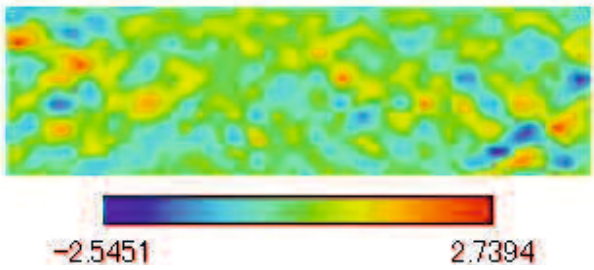

(d) Specimen no.2B

Fig. 3.6 Contour maps of stress distribution in 3-1-direction

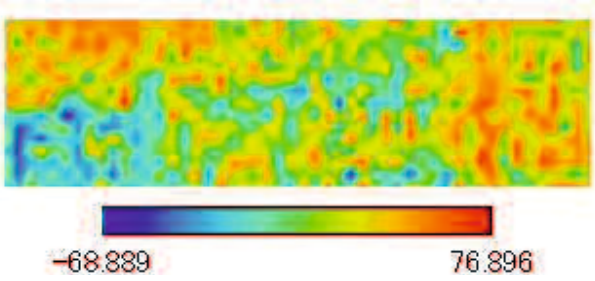

(a) Specimen no.1A

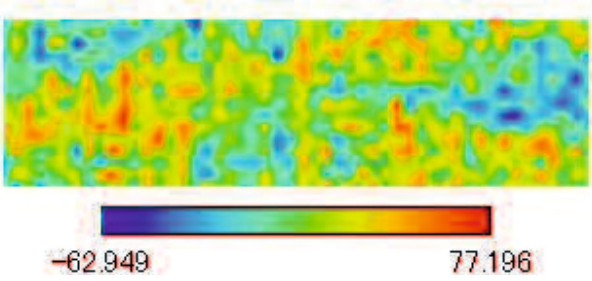

(b) Specimen no.1B

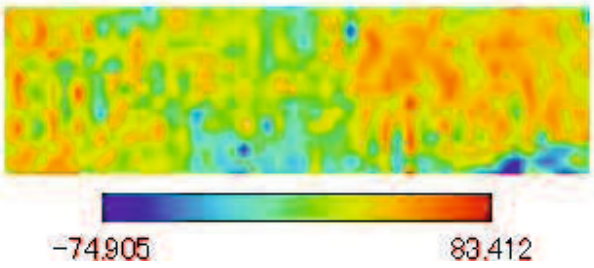

(c) Specimen no.2A

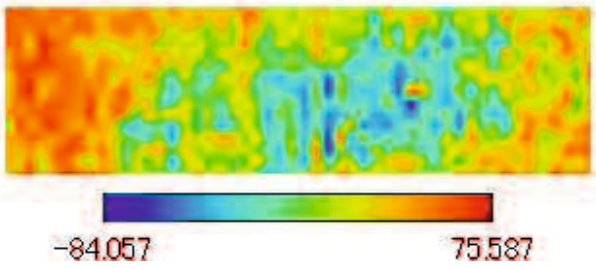

(d) Specimen no.2B

Fig. 3.7 Contour maps of stress distribution in 1-2-direction

To define the effect of tensile stresses on specimens, the maximum stress in direction 1, 2 and 3 was selected, and then the stresses in direction 1, 2 and 3 were divided by the maximum stress. In addition, the shear stresses in direction in 23, 31 and 12 were divided by the maximum shear stresses. The maximum tensile stresses are 445.645MPa and 442.516MPa and the maximum shear stresses are 77.196MPa and 83.412MPa for the specimen no.1 and 2.

As the results of the tensile stresses in figs.3.8 and 3.9, the red areas (the high stress) in the stress direction 1 and 2 but it doesn't appear in the direction3. Thus, we are able to ignore the tensile stress in direction 3 for the failure criterion. Likewise, the results of the shear stresses in figs.3.10 and 3.11, the red areas only appear in the shear stress direction12. Thus, the shear stresses in direction 23 and 31 are ignored for the failure criteria in the next chapter.

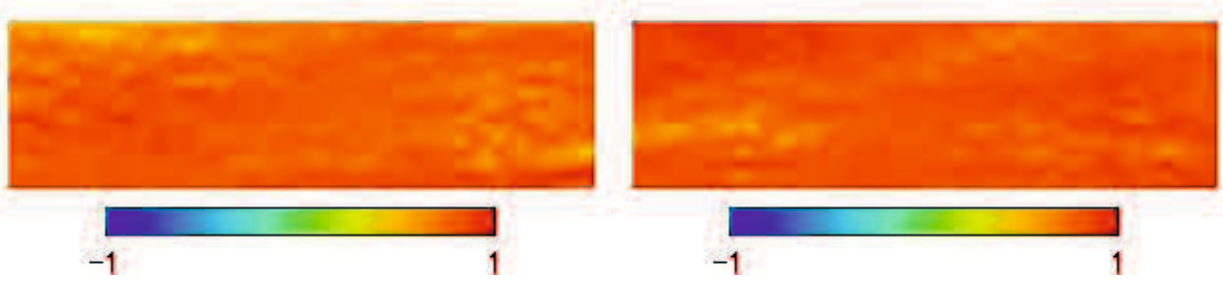

(a) Tensile stress direction2 on side A and B respectively

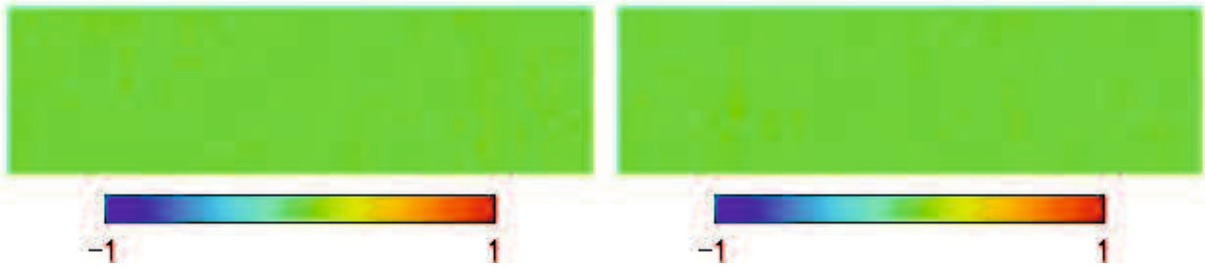

(b) Tensile stress direction1 on side A and B respectively

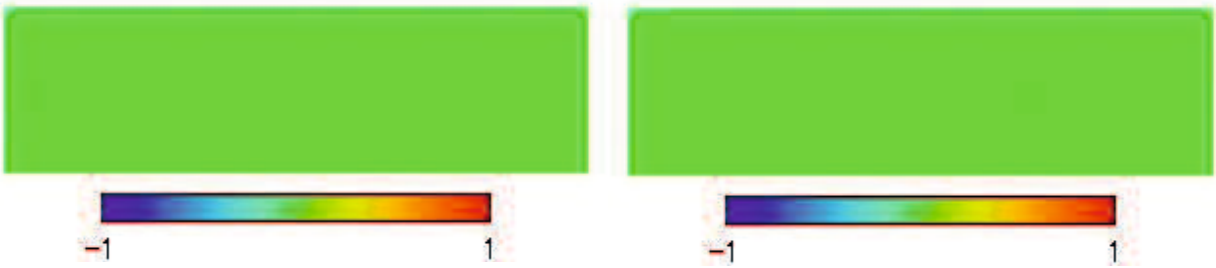

(c) Tensile stress direction3 on side A and B respectively

Fig. 3.8 Contour maps of tensile stress distribution in 1-2-3-direction on specimen no.1

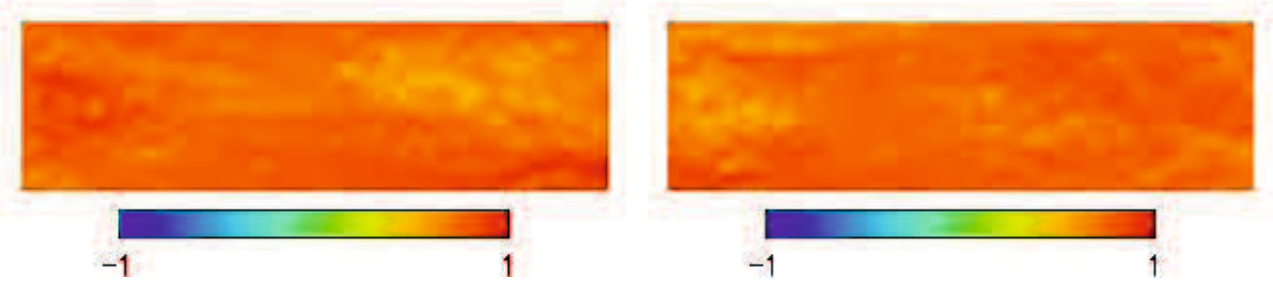

(a) Tensile stress direction2 on side A and B respectively

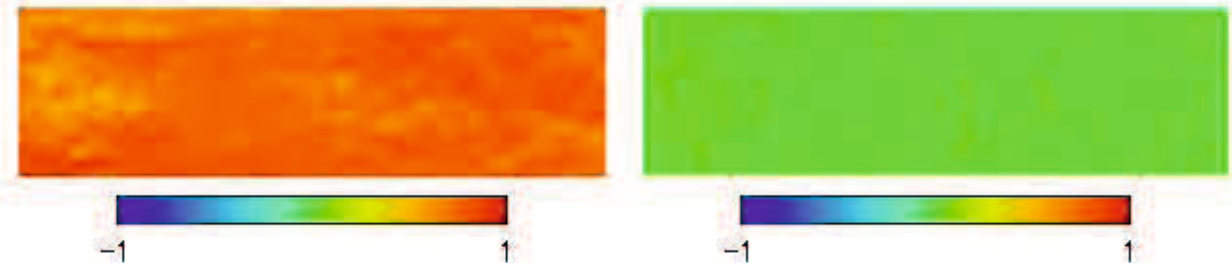

(b) Tensile stress direction1 on side A and B respectively

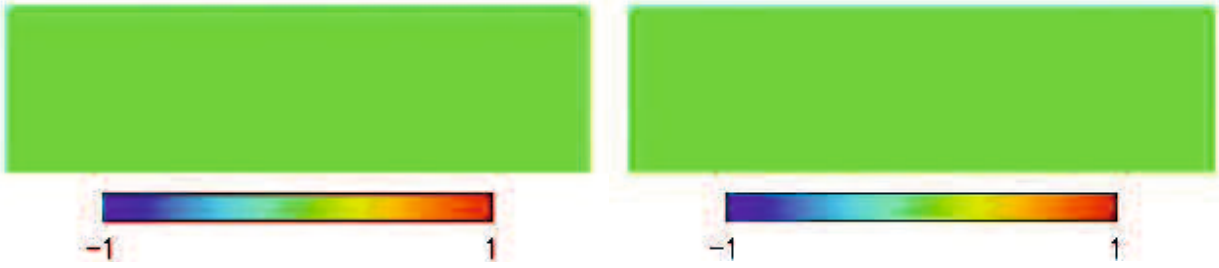

(c) Tensile stress direction3 on side A and B respectively

Fig. 3.9 Contour maps of tensile stress distribution in 1-2-3-direction on specimen no.2

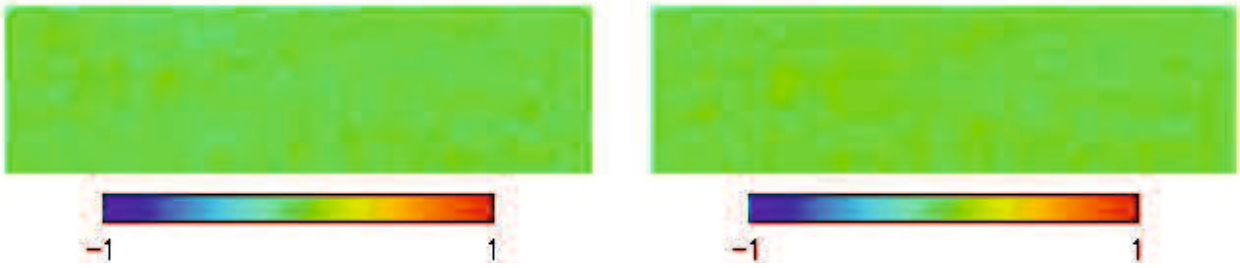

(a) Shear stress direction23 on side A and B respectively

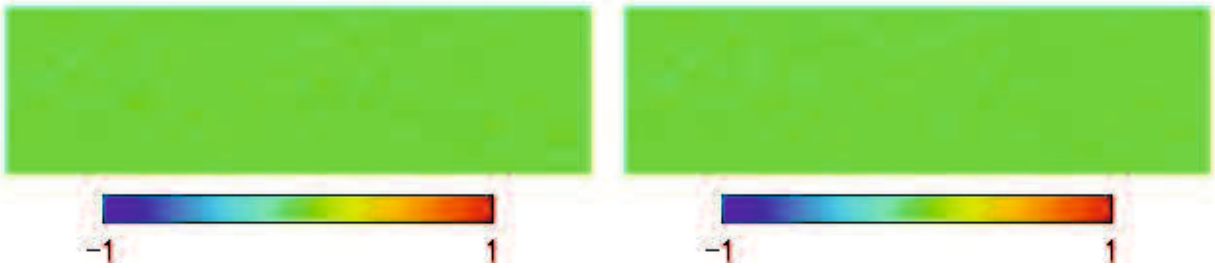

(b) Shear stress direction31 on side A and B respectively

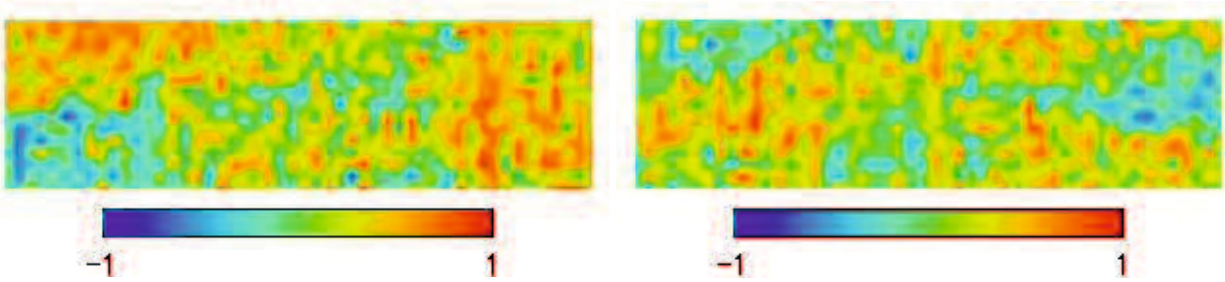

(c) Shear stress direction12 on side A and B respectively

Fig. 3.10 Contour maps of shear stress distribution in 23, 31 and 12 direction on specimen no.1

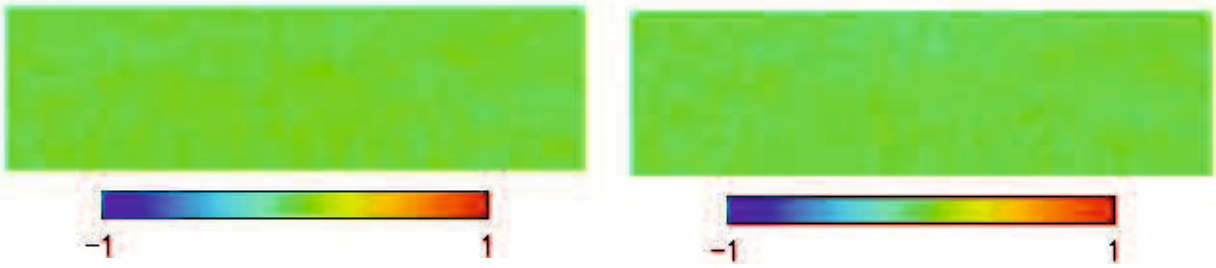

(a) Shear stress direction23 on side A and B respectively

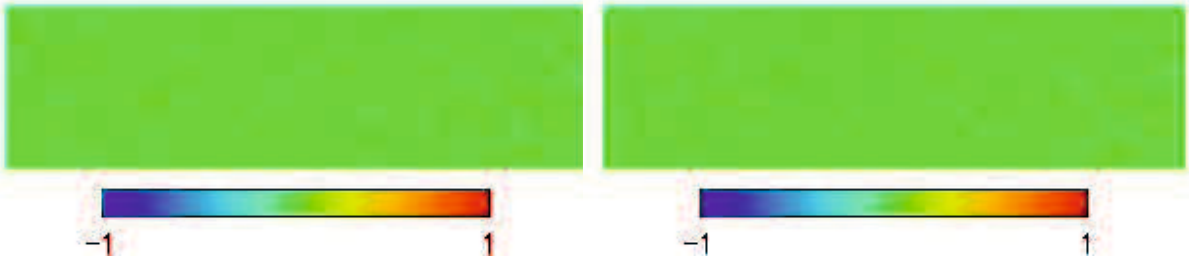

(b) Shear stress direction31 on side A and B respectively

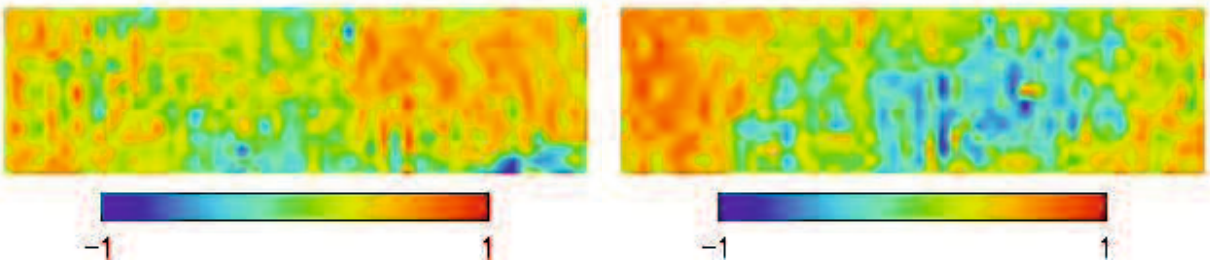

(c) Shear stress direction12 on side A and B respectively

Fig. 3.11 Contour maps of shear stress distribution in 23, 31 and 12 direction on specimen no.2

As the result of specimen 1A from the finite element method, stresses (σ_y) following the loading direction trend to decrease with the angle distributions on the specimens in fig.3.12. It means the high angle distribution on specimens affect the tensile stress.

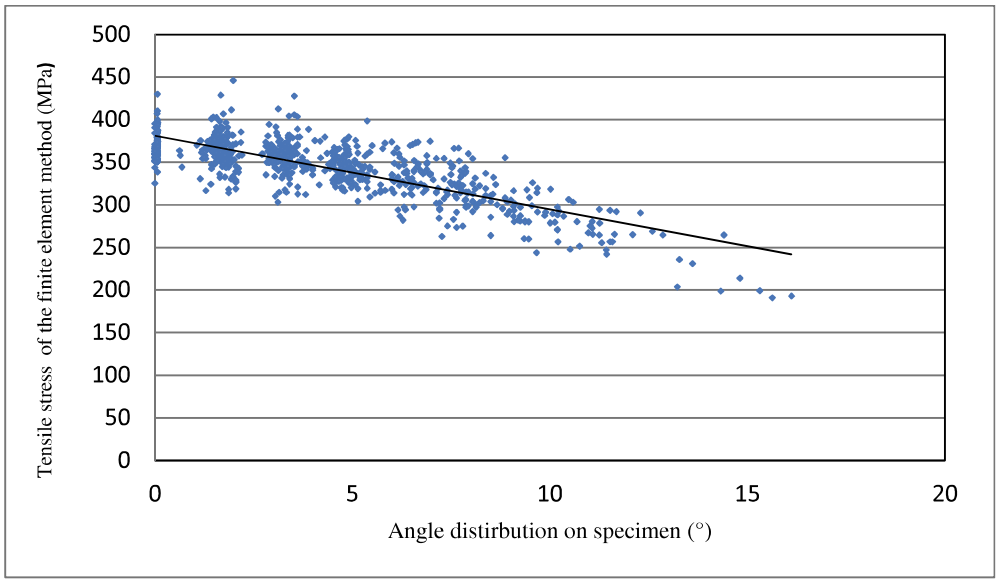

Fig.3.12 Relation between the tensile stress followed loading direction and the angle distribution on specimens

3.4 Conclusions

In this chapter, the finite element method was to analyze the tensile and shear stresses on a flax fiber-reinforced composite. The red areas are the high effect of stress which trend to be the risky areas on the specimen. From the ratio of the tensile stress divided by the maximum stress in direction 1,2 and 3, the red areas appear in the stresses direction 1 and 2 but it doesn't appear in direction 3. As the ratio of shear stresses in the direction 23, 13 and 12, the red areas only appear

in the direction 12 but it doesn't appear in the direction 23 and 13. Thus, the tensile stress in direction3 and the shear stress in direction 23 and 13 are negligible for the failure criteria.

Regarding the results of the finite element method, stresses following the loading direction (σ_y) trend to decrease with the angle distributions on the specimens. It means the high angle distribution on specimens affect the tensile stress.

Chapter IV The effect of random fiber waviness on damage and fracture properties of a natural fiber sliver-reinforced composite

4.1 Introduction

In the field of textile industry, so-called 'sliver' is the initial form of textile products, which is obtained by combing a bunch of plant-based natural fibers. Spun yarns, the final product, are then obtained through the spinning process of the sliver. Sliver is not twisted macroscopically, so that this 'continuous' form is quite convenient when we use it as a reinforcing material. But, sliver often exhibits fiber waviness which is inherent in the natural fibers. Because the shape of plant-based natural fibers is complicated and statistically varies, fiber waviness is caused by entanglement between individual fibers in the sliver.

In this study, the effect of random fiber waviness on damage and fracture properties of a natural fiber sliver-reinforced composite was clarified through finite element method (FEM) and spatial analysis. First of all, fiber waviness was quantified. The composite surface was divided by 1mm x 1mm squares, and the fiber orientation angles to the loading direction were measured on the all squares. Finite element analysis was carried out by recognizing the divided squares as finite elements. Stress-strain relation of the finite element was based on the orthotropic theory, in which the measured angles were assigned to each element. In order to predict risky areas causing damage in the composite, Tsai-Hill criterion was applied for the resultant stress distribution. On the other hand, if the applied stress is given to each element, Tsai-Hill criterion can be applied for the all elements without using FEM. This means, each element exists isolatedly without any interaction between elements in a composite. Such a Tsai-Hill criterion value without FEM is denoted as angle-based Tsai-Hill. After such calculations with and without FEM were done,

relatively high FEM-based and angle-based Tsai-Hill values were picked up and compared. When a FEM-based Tsai-Hill value is higher than the corresponding angle-based Tsai-Hill, we consider that damage is accelerated by interaction brought from the fiber waviness. In other word, this element is placed under sensitive interaction. On the contrary, when the angle-based Tsai-Hill is higher, this element is not under sensitive interaction although it might originally be risky. From the angle distribution at the risky areas, one is the high angle distribution but it is still smooth angle from the surrounding areas. Another is high angle and the angle is disordered from the surrounding areas.

Thus, the subtraction of Tsai-Hill without FEM value from Tsai-Hill value was done for each element, and the elements giving the positive maximum and negative maximum differences were picked up. For such elements and surrounding elements, the coefficients of variation (C.V.) of the element angles were calculated. Results showed that the C.V. of the element angles giving the positive maximum difference is larger than C.V. of the angles of the negative maximum difference. Such tendency was confirmed for almost all specimens. This means, the sensitive interaction of fiber waviness is caused by variation in element angle, while the insensitive interaction is brought from a group of relatively uniform angle elements.

4.2 Analytical method

To evaluate damage area in the composites with fiber waviness, furthermore, damage risk points in the specimen were predicted using Tsai-Hill criterion.

4.2.1 Tsai-Hill criterion

In this study, two-dimensional Tsai-Hill criterion was applied for predicting the risky areas on specimens because the tensile stresses in the direction 3 are very small compared with the stress in the direction 1 and 2. Likewise, the shear stresses in direction 13 and 23 are very small compared with the shear strength in the direction12. Thus, the tensile stress in direction 3 and the shear stresses in the direction 13 and 23 are negligible. Thus, two-dimension Tsai-Hill criterion is enough to predict the failure on specimens.

The stress in the direction 2 along the fiber direction, stress in the direction 1 transverse with the fiber direction and the shear stress were calculated at each element using the finite element analysis. Then, Tsai-Hill criterion was applied for definition of risky areas on the specimen. The stresses at each element are influenced by the interaction between elements. For this influence, σ_1, σ_2 and τ_{12} were the major stress components, so in this study Tsai-Hill criterion was reduced as the following:

$$\left(\frac{\sigma_1}{S_1}\right)^2 - \frac{\sigma_1\sigma_2}{{S_2}^2} + \left(\frac{\sigma_2}{S_2}\right)^2 + \left(\frac{\tau_{12}}{S_{12}}\right)^2 = 1 \qquad (1)$$

where, S_2 is the longitudinal strength, S_1 is the transverse strength, S_{12} is the shear strength.

4.2.2 Tsai-Hill criterion without FEM

This method does not require the stresses on each element thus this criterion is calculated by one stress direction along Y-axis. It means the interaction between fibers have not affected with this method, thus the high coefficients rely on each segment of the angle distribution. Tsai-Hill criterion without FEM is denoted as Tsai-Hill without FEM and calculated as:

$$\left(\frac{\cos^4\theta}{{S_1}^2}+\left[\frac{1}{{S_3}^2}-\frac{1}{{S_1}^2}\right]\cos^2\theta\sin^2\theta+\frac{\sin^4\theta}{{S_2}^2}\right)*{\sigma_x}^2=1 \qquad (2)$$

4.3 Results and discussions

4.3.1 Tsai-Hill criterion and Tsai-Hill criterion without FEM

This study aims to analyze the effect of random fiber waviness on the tensile strength of sliver-based natural fiber composites. The fiber waviness was initially quantified by the fiber orientation angles. The Fiber orientation angles have a broad range of positive twenty degrees to negative twenty degrees. The contour maps of fiber orientation angles (specimen no.1A, 2A, 3A and 4A) are shown in figures 4.1 (a), (b), (c) and (d) respectively. As the results of Tsai-Hill criterion and Tsai-Hill criterion without FEM in fig.4.2 and fig.4.3, the red color means the weakest point of the specimen.

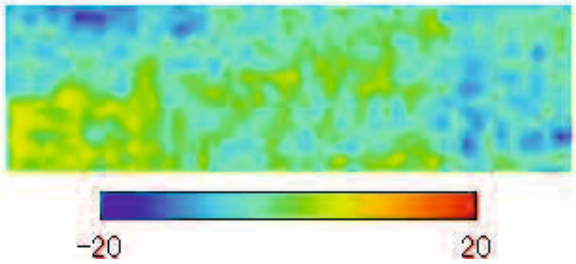

(a) Specimen 1A

($\bar{\theta}$: 3.30°, standard deviation: 4.28°)

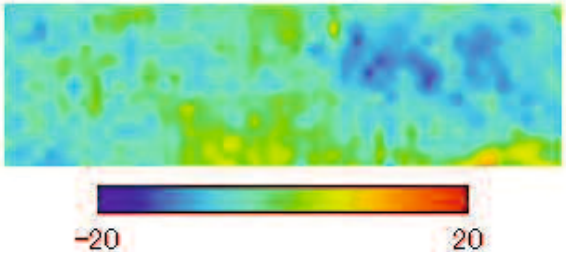

(b) Specimen 2A

($\bar{\theta}$: 4.19°, standard deviation: 4.03°)

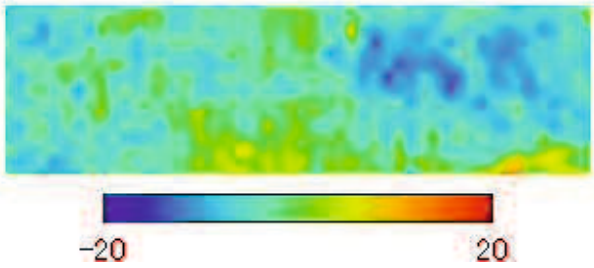

(c) Specimen 3A

($\bar{\theta}$: 5.14°, standard deviation: 4.06°)

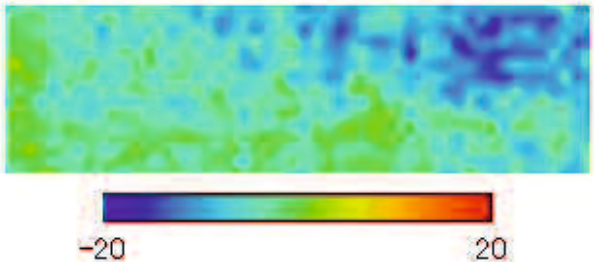

(d) Specimen 4A

($\bar{\theta}$: 3.05°, standard deviation: 3.22°)

Fig. 4.1 Contour map of fiber orientation angle distribution

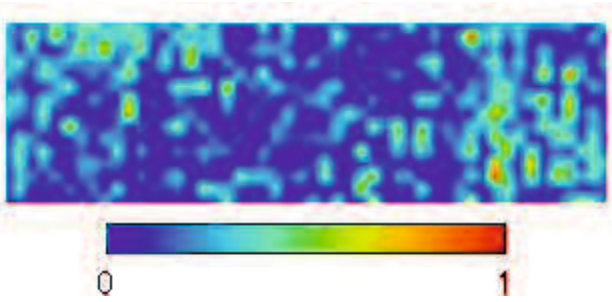

(a) Tsai-Hill criterion based on measured angles of Fig.4.1 (a)

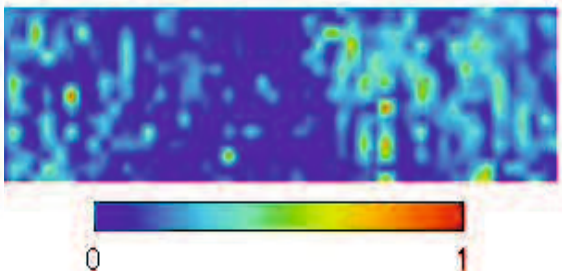

(b) Tsai-Hill criterion based on measured angles of Fig.4.1(b)

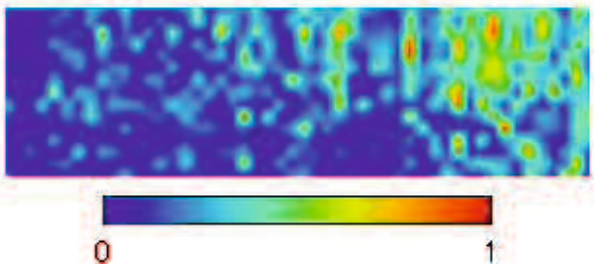

(c) Tsai-Hill criterion based on measured angles of Fig.4.1 (c)

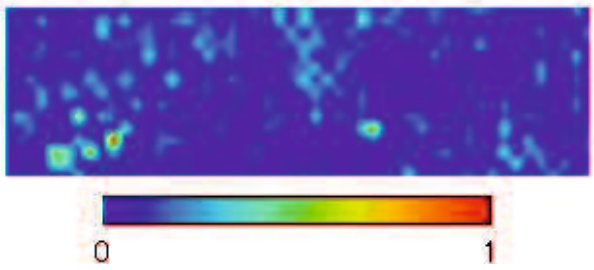

(d) Tsai-Hill criterion based on measured angles of Fig.4.1(d)

Fig. 4.2 Contour map of Tsai-Hill criterion

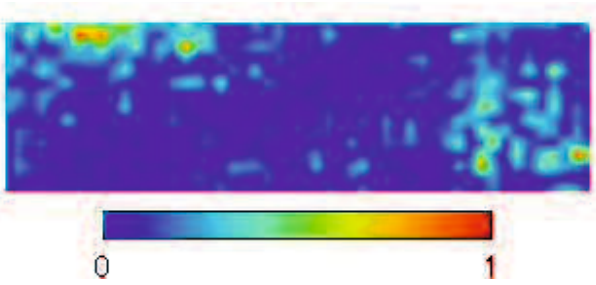

(a) Tsai-Hill criterion without FEM based on measured angles of Fig.4.1 (a)

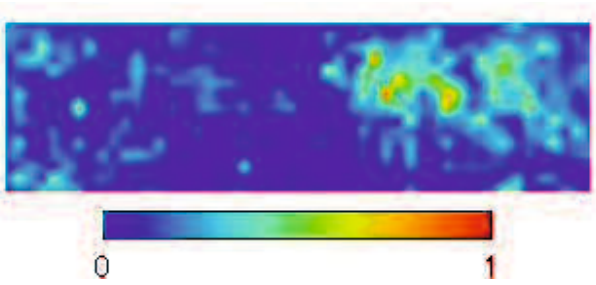

(b) Tsai-Hill criterion without FEM based on measured angles of Fig.4.1(b)

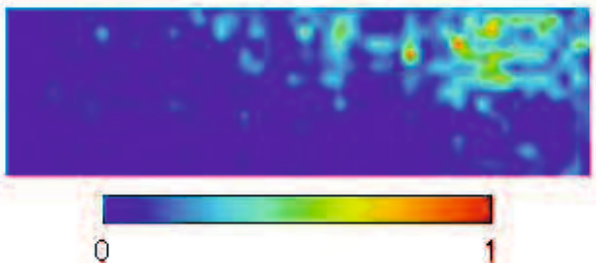

(c) Tsai-Hill criterion without FEM based on measured angles of Fig.4.1 (c)

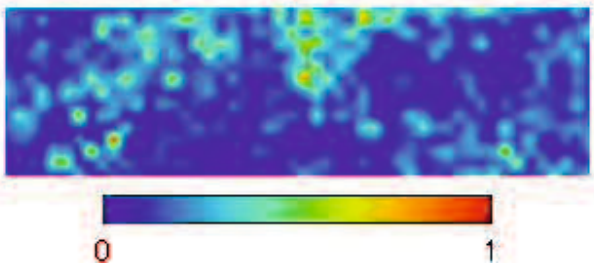

(d) Tsai-Hill criterion without FEM based on measured angles of Fig.4.1(d)

Fig. 4.3 Contour map of Tsai-Hill criterion without FEM

4.3.2 Relation between the weigh function of Local Geary's *c* and Tsai-Hill criterion

Normally, the results between Local Geary's *c* and Tsai-Hill criterion are nearly the same at the risky areas because both methods use the data between that position and neighbor positions. Accordingly, the first method uses the angle distribution around the neighbor areas and the second method uses the stresses distribution between the elements to calculate the risky area.

In fig. 4.12, 4.13 and 4.14 show that high coefficient of Local Geary's *c* moves to high coefficient of Tsai-Hill criterion when increasing the weigh function of Local Geary's *c*. Thus, Local Geary's *c* with the suitable weigh function is able to predict the risk points on the specimens without using the finite element method.

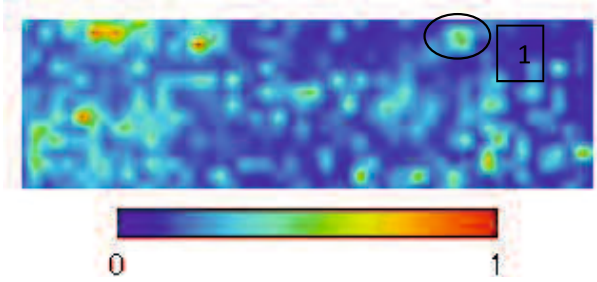

(a) Local Geary's *c* with weigh function 1

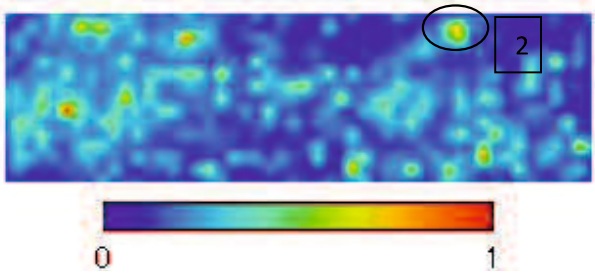

(b) Local Geary's *c* with weigh function 2

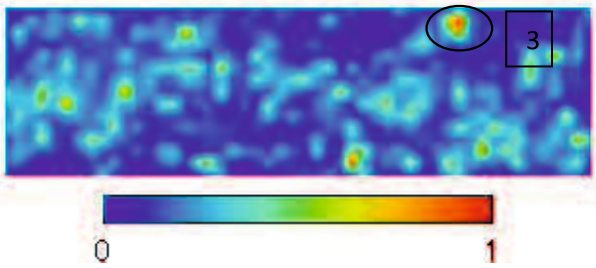

(c) Local Geary's *c* with weigh function 3

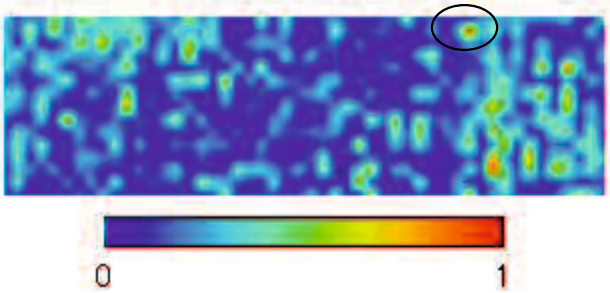

(d) Tsai-Hill criterion

Fig.4.12 Relation between the weigh function of Local Geary's *c* and Tsai-Hill criterion on specimen no.1A

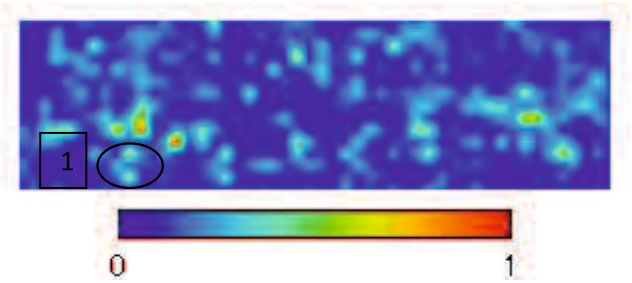

(a) Local Geary's *c* with weigh function 1

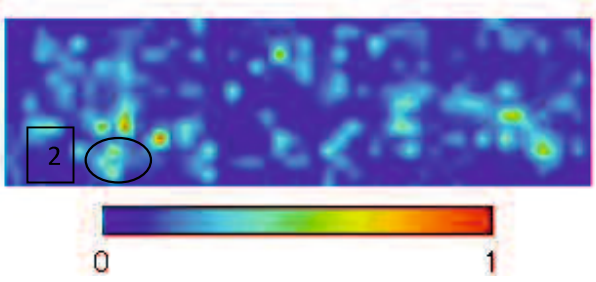

(b) Local Geary's *c* with weigh function 2

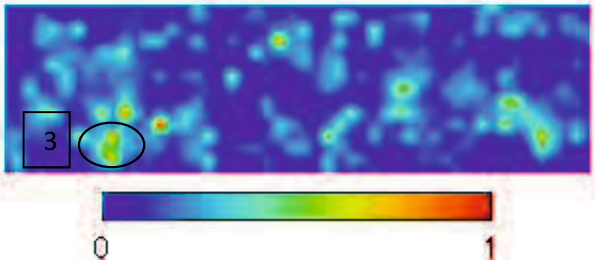

(c) Local Geary's *c* with weigh function 3

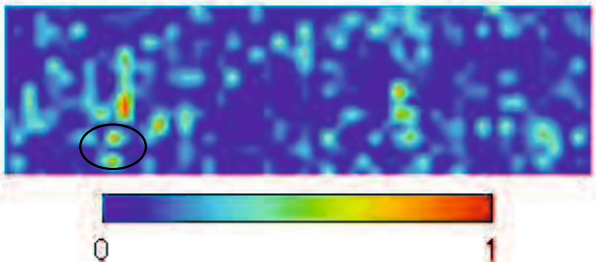

(d) Tsai-Hill criterion

Fig.4.13 Relation between the weigh function of Local Geary's *c* and Tsai-Hill criterion on specimen no.1B

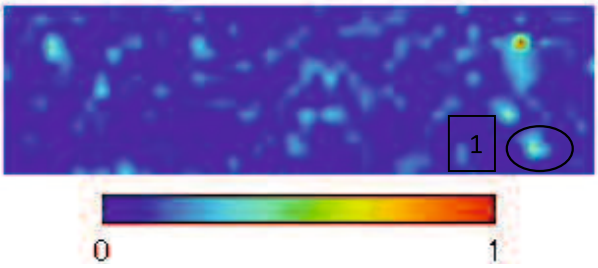

(a) Local Geary's *c* with weigh function 1

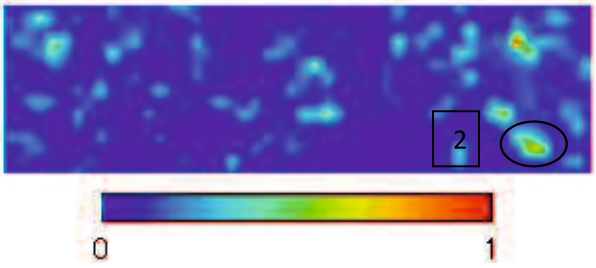

(b) Local Geary's *c* with weigh function 2

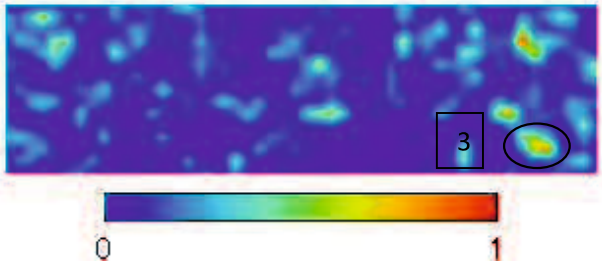

(c) Local Geary's *c* with weigh function 3

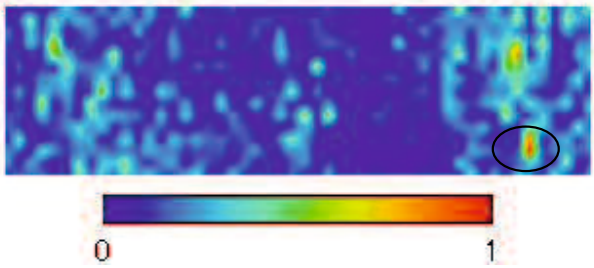

(d) Tsai-Hill criterion

Fig.4.14 Relation between the weigh function of Local Geary's *c* and Tsai-Hill criterion on specimen no.3B

4.3.3 The surrounding angles at FEM-based Tsai-Hill and angle-based Tsai-Hill analyses

In order to clarify physical meanings of Tsai-Hill criterion and Tsai-Hill criterion without FEM, one indicator was defined as delta in equation 3.

$$\text{delta}(i) = \text{Tsai-Hill criterion } (i) - \text{Tsai-Hill criterion without FEM } (i) \qquad (3)$$

This is the difference between Tsai-Hill criterion and Tsai-Hill criterion without FEM values at *i*-th element on a specimen. First, we extracted two elements giving the maximum and the minimum deltas from one-side of a specimen. Next, Tsai-Hill criterion (the maximum delta) was defined as FEM-based Tsai-Hill analyses, and Tsai-Hill without FEM criterion (the minimum delta) was defined as Angle-based Tsai-Hill analyses. Later, we calculated averages and coefficient of variations of eight element angles around the extracted two elements. In this calculation the element angles giving the maximum and minimum deltas were taken into account. Results show in Table 4.1 that, in any case, the coefficients of variation (C.V.) of the maximum delta group are much higher in absolute value than that of the minimum delta group, whereas the averages of the former are less in absolute value than the latter. This means, the maximum delta group given by a higher FEM-based Tsai-Hill value encounters strict interaction between fiber orientations, despite of less average angles in absolute value. It is interpreted that such a strict interaction enhances the corresponding Tsai-Hill value. On the other hand, the minimum delta group given by a less angle-based Tsai-Hill value consists of a cluster of inclined fibers. Little interaction between fiber orientations works, but the inclined fibers increase the corresponding Tsai-Hill value. Thus, we understand that FEM-based and angle-based Tsai-Hill analyses give two kinds of geometric meanings in fiber waviness.

Table 4.1 Surrounding angles at the Tsai-Hill criterion defined by deltas

No.	Delta	Angle patterns(°)			Avg.(°)	S.D. (°)	CV.
1A	-1.000	-10.513	-11.070	-12.095	-10.839	2.921	-0.269
		-7.792	-16.113	-14.323			
		-8.043	-9.560	-8.043			
	0.904	-1.637	-2.045	-6.864	-2.580	5.443	-2.110
		3.991	-11.070	-8.130			
		2.921	3.668	-4.050			
1B	-0.559	-7.481	-1.601	-3.382	-7.119	3.304	-0.464
		-9.522	-10.627	-10.958			
		-8.596	-7.549	-4.357			
	1.000	1.535	1.460	1.838	-1.602	4.178	-2.608
		0.000	-7.316	3.460			
		-4.373	-7.691	-3.333			
2A	-0.677	-10.899	-8.774	-14.816	-10.614	2.997	-0.282
		-7.481	-16.138	-8.725			
		-8.560	-9.059	-11.073			
	0.886	-11.073	-8.424	-6.817	-7.098	2.793	-0.393
		-3.421	-11.371	-4.784			
		-7.407	-6.000	-4.586			
2B	-0.907	-8.475	-6.906	-10.266	-10.171	2.792	-0.274
		-11.029	-15.512	-7.534			
		-9.636	-13.395	-8.791			
	1.000	0.000	9.689	-5.572	0.635	5.551	8.746
		-5.572	9.039	0.000			
		-3.252	1.380	0.000			
3A	-0.275	-19.799	-11.860	-11.434	-13.353	3.137	-0.235
		-13.496	-15.945	-13.276			
		-9.942	-9.942	-14.480			
	1.000	-9.187	-6.665	-5.009	-4.821	3.554	-0.737
		0.000	-9.118	0.000			
		-1.673	-5.009	-6.729			
4A	-1.000	-6.706	-7.199	-9.501	-6.935	2.651	-0.382
		-6.051	-11.684	-5.711			
		-2.490	-5.024	-8.053			
	0.467	-0.836	-1.487	0.000	1.757	5.253	2.990
		-1.628	-6.426	5.820			
		2.361	8.829	9.181			

4.3.4 Risky areas of FEM-based Tsai-Hill and angle-based Tsai-Hill analyses

To identify risky areas connecting to fracture of the laminate specimens, FEM-based and angle-based Tsai-Hill analyses were compared. For the elements with the positive delta, i.e. delta(i) > 0.5, we re-plotted the contour maps of FEM-based Tsai-Hill analyses. And, for the elements with the negative delta, i.e. delta(i) < -0.1, we re-plotted the contour maps of angle-based Tsai-Hill analyses. The results are shown in Figs. 4.15 (b)(c)(d)(e) and 4.16(b)(c)(d)(e) for specimens 1 and 2, respectively. In Figs. 4.15(a) and 4.16(a), the fractured specimens are also shown. From comparison between these figures, it is proved that both angle-based Tsai-Hill analyses in Figs. 4.15(d) and 4.16(d) contain a part of the fracture paths, as shown in the solid circles. On the other hand, it is hard to identify the paths from the contour map of FEM-based Tsai-Hill analyses in Figs. 4.15(b)(c) and 4.16(b)(c). It seems that, therefore, the risky area connecting to fracture is given by angle-based Tsai-Hill analyses.

Here, one question is rising in this context, that is, why angle-based Tsai-Hill analyses can predict the fracture initiation, despite that it does not analyze the actual stress distribution. Let us remind that the minimum delta group was a cluster of inclined fibers. Usually, inclined fibers cannot sustain the applied tensile load so much. In other words, the extra load has to be sustained by another lamina. Figs. 4.15(f)(g) and 4.16(f)(g) show the contour maps of tensile stress σ_2 along fiber-axis. Less tensile stress σ_2 area is shown in blue, and higher area is in red or orange. As easily known from the solid circles on these figures, red or orange areas in a lamina appear in the blue areas in another lamina. It is guessed that such biased stress distribution induces the fibers' breakage, and results in the whole fracture. As known from Figs. 4.15(b)(c) and 4.16(b)(c), the contour maps of FEM-based Tsai-Hill analyses do not appear with clusters, and rather does with dispersion. These look small-scale defects, but can be interpreted as a

positive effect of interaction between fiber orientations because of the dispersion and small size. Thus, we can conclude that FEM-based Tsai-Hill analyses is not enough in predicting damage and fracture of fibrous composites with random fiber waviness. Moreover, it was confirmed with the specimen no.5 and 10 in Figs. 4.17 and 4.18.

(a) Fractured specimen

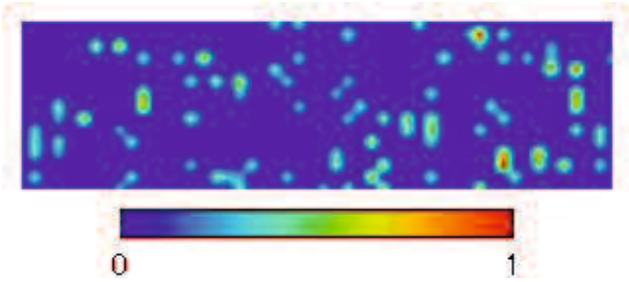

(b) Contour map of FEM-based Tsai-Hill analyses on specimen no.1A

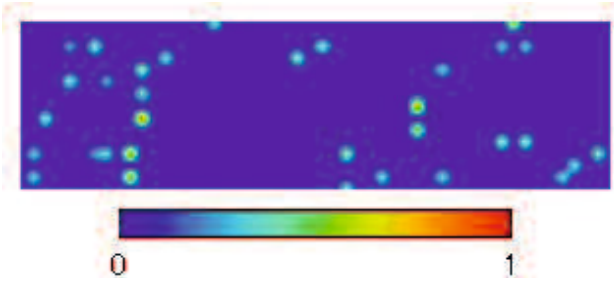

(c) Contour map of FEM-based Tsai-Hill analyses on specimen no.1B

(d) Contour map of angle-based Tsai-Hill analyses on specimen no.1A

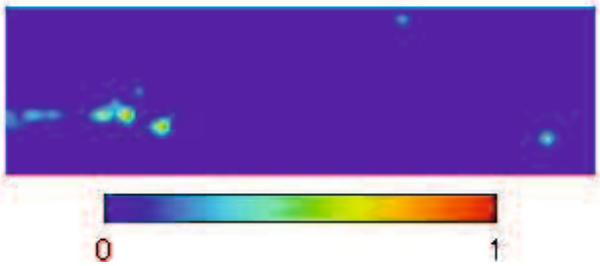

(e) Contour map of angle-based Tsai-Hill analyses on specimen no.1B

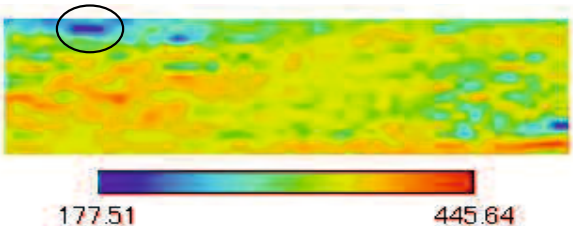

(f) Contour map of σ_2 distribution on specimen 1A

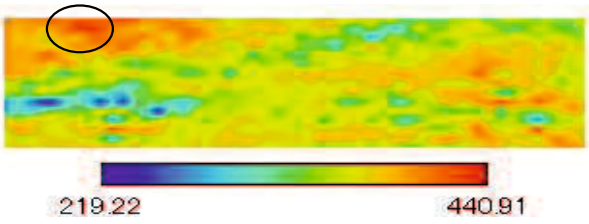

(g) Contour map of σ_2 distribution on specimen 1B

Fig. 4.15 Defective area on specimen no.1 defined by FEM-based Tsai-Hill and angle-based Tsai-Hill analyses

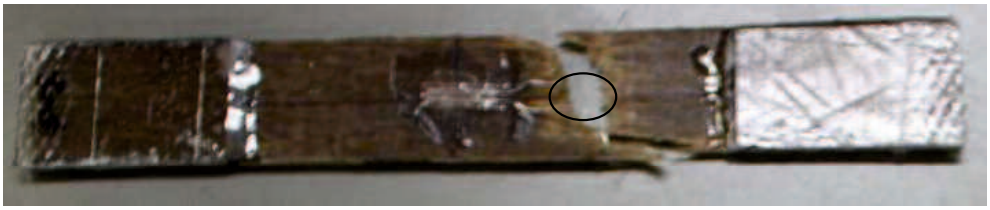

(a) Fractured specimen

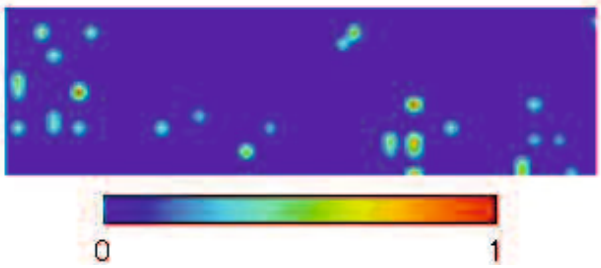

(b) Contour map of FEM-based Tsai-Hill analyses on specimen no.2A

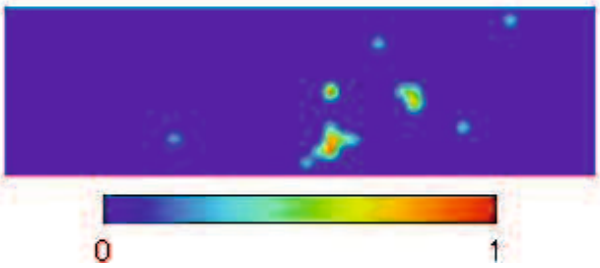

(c) Contour map of FEM-based Tsai-Hill analyses on specimen no.2B

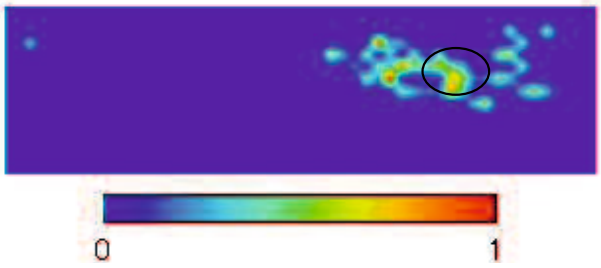

(d) Contour map of angle-based Tsai-Hill analyses on specimen no.2A

(e) Contour map of angle-based Tsai-Hill analyses on specimen no.2B

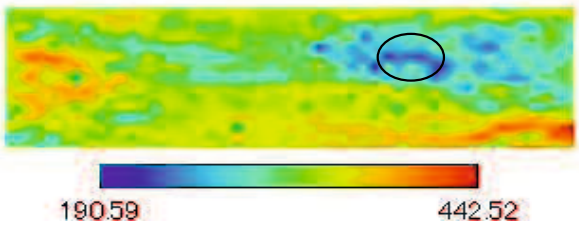

(f) Contour map of σ_2 distribution on specimen 2A

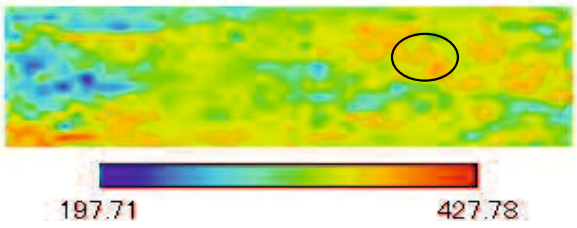

(g) Contour map of σ_2 distribution on specimen 2B

Fig. 4.16 Defective area on specimen no.2 defined by FEM-based Tsai-Hill and angle-based Tsai-Hill analyses

(a) Fractured specimen

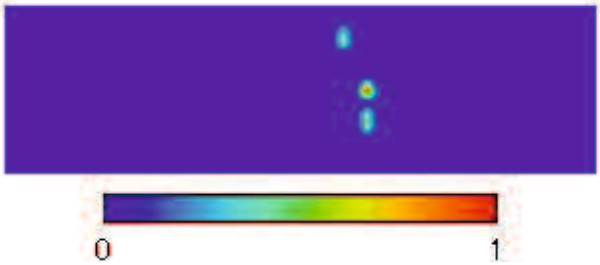

(b) Contour map of FEM-based Tsai-Hill analyses on specimen no.5A

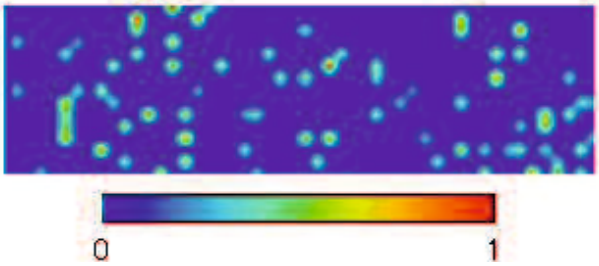

(c) Contour map of FEM-based Tsai-Hill analyses on specimen no.5B

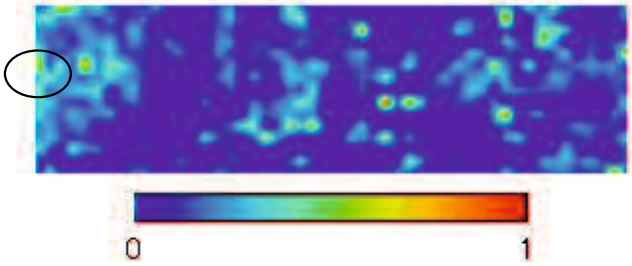

(d) Contour map of angle-based Tsai-Hill analyses on specimen no.5A

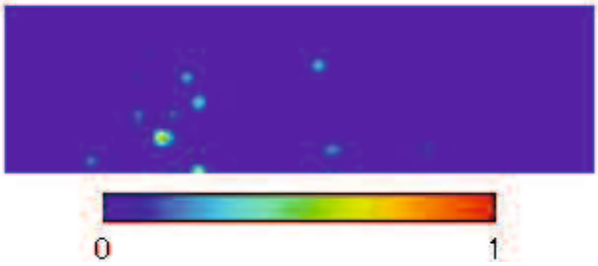

(e) Contour map of angle-based Tsai-Hill analyses on specimen no.5B

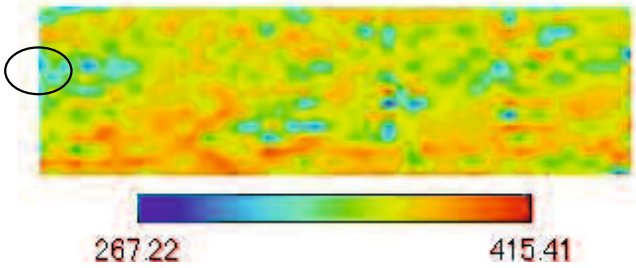

(f) Contour map of σ_2 distribution on specimen 2A

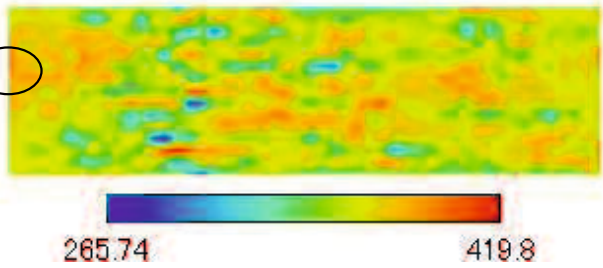

(g) Contour map of σ_2 distribution on specimen 2B

Fig. 4.17 Defective area on specimen no.5 defined by FEM-based Tsai-Hill and angle-based Tsai-Hill analyses

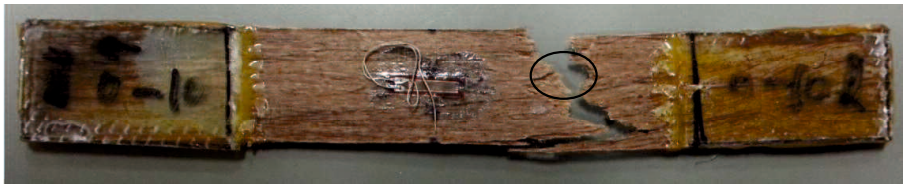

(a) Fractured specimen

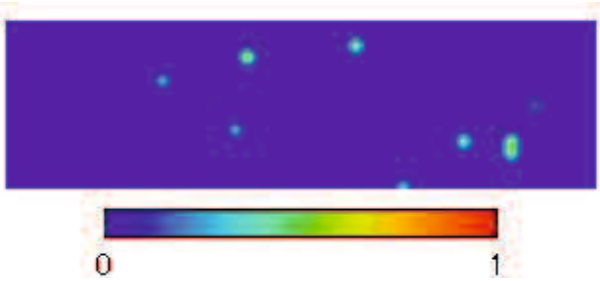

(b) Contour map of FEM-based Tsai-Hill analyses on specimen no.10A

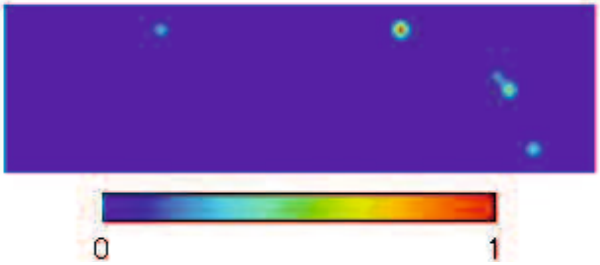

(c) Contour map of FEM-based Tsai-Hill analyses on specimen no.10B

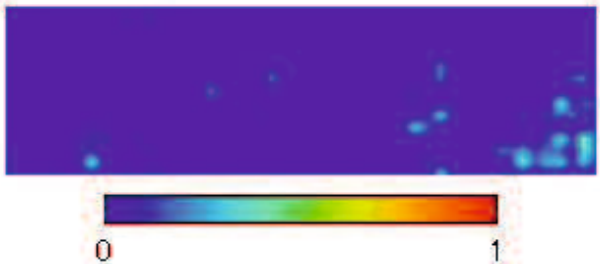

(d) Contour map of angle-based Tsai-Hill analyses on specimen no.10A

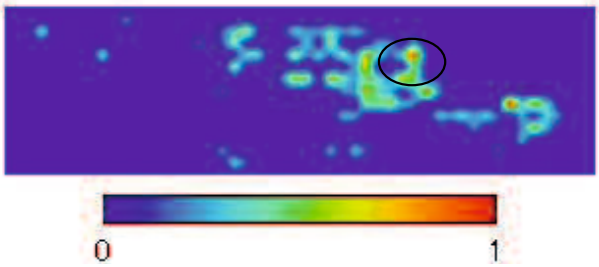

(e) Contour map of angle-based Tsai-Hill analyses on specimen no.10B

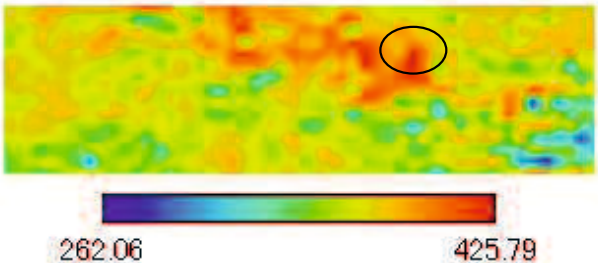

(f) Contour map of σ_2 distribution on specimen 2A

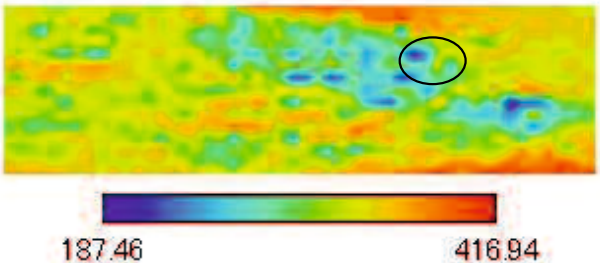

(g) Contour map of σ_2 distribution on specimen 2B

Fig. 4.18 Defective area on specimen no.10 defined by FEM-based Tsai-Hill and angle-based Tsai-Hill analyses

4.4 Conclusions

In this study, we aim to analyze the effect of random fiber waviness on the tensile strength of sliver-based natural fiber composites. Thus, FEM-based Tsai-Hill and angle-based Tsai-Hill analyses were analyzed the fiber waviness. As, Tsai-Hill (TH) criterion was applied to predict risky damage areas in the composite laminate. This criterion can predict the degree of damage caused by interaction between fiber orientations. On the other hand, TH distribution without finite element method was also estimated by giving an applied stress to each element, to which only a measured fiber orientation angle was respectively assigned. Such calculated TH distribution corresponded approximately to the degree of fiber orientation angles. To differentiate the two kinds of Tsai-Hill criterion distribution, the subtraction of the latter value from the former was taken for each element. In the negative subtraction (angle-based Tsai-Hill analysis's area), risky Tsai-Hill distributions were estimated, in case there was an area consisting of a cluster of inclined fibers in the composite laminate. In the positive subtraction (FEM-based Tsai-Hill analysis's area), on the other hand, risky Tsai-Hill distributions appear with dispersion and small-scale level. From the comparison with the specimens' fracture paths, the fracture initiation was estimated to occur from the cluster, but not from FEM-based Tsai-Hill analysis's area. Finally, we concluded that, the fracture was not initiated from the cluster, but it was caused by fibers breakage on the counterpart in the laminate because of tensile stress enhancement induced by the cluster of inclined fibers.

Regarding the relation between Local Geary's c and FEM-based Tsai-Hill analyses, Local Geary's c with the suitable weigh function is able to identify the risky points of FEM-based Tsai-Hill analyses. Thus, Local Geary's c is another method to predict the risky points, and it has less equation and does not take a long time for creating the program.

Chapter V Summary

Fiber waviness of a flax sliver-reinforced composite material was studied. Based on the results of the present study, the conclusions can be summarized as follows.

In Chapter II, the fiber waviness was quantified using Local Moran's *I* and Local Geary's *c*, both of which were able to express the degree of disorder in fiber orientation. The results show that Local Moran's *I* is correlated well with tensile strength of the composite specimens when appropriate threshold levels are selected. On the other hand, Local Geary's *c* is not well correlated with tensile strength. Thus, the area ration of Local Moran's *I* proposed in this study is an effective tool of predicting roughly the tensile strength of natural-fiber-sliver-based composite materials.

In Chapter III, three-dimensional finite element method was used for calculating stress distribution of the sliver-based green composite. As the results of the finite element method, the red areas of the contour map are the high effect of stress. From the ratio of the tensile stresses divided by the maximum stresses in direction 1, 2 and 3, the red areas appear in the stresses direction 1 and 2 but it doesn't appear in direction 3. As the ratio of shear stresses in the direction 23, 13 and 12, the red areas only appear in the direction 12 but it doesn't appear in the direction 23 and 13. Thus, the tensile stress in direction3 and the shear stresses in direction 23 and 13 are negligible for the failure criteria. Regarding the results of the finite element method, stresses following the loading direction (σ_y) trend to decrease with the angle distributions on the specimens. It means the high angle distribution on specimens affect the tensile strength.

In Chapter IV, the risky areas of fiber waviness on the tensile strength of sliver-based natural fiber composites were analyzed by FEM-based Tsai-Hill and angle-based Tsai-Hill analyses. The different between FEM-based Tsai-Hill and angle-based Tsai-Hill analyses were classified by the coefficient of variation (C.V.) of the angle patterns. The high coefficient of FEM-based Tsai-Hill analyses shows that the cv. of angle pattern is higher than the cv. of angle pattern at the high coefficient of angle-based Tsai-Hill analyses at the same side. It means the angle pattern of FEM-based Tsai-Hill analyses depends on the high distribution of angles. On the other hand, the high coefficient of angle-based Tsai-Hill analyses depends on the declination angle on the specimens.

From the comparison with the specimens' fracture paths, the fracture initiation was estimated to occur from the cluster, but not from FEM-based Tsai-Hill analysis's area. Finally, we concluded that, the fracture was not initiated from the cluster, but it was caused by fibers breakage on the counterpart in the laminate because of tensile stress enhancement induced by the cluster of inclined fibers.

Regarding the relation between Local Geary's *c* and Tsai-Hill criterion, Local Geary's *c* with the suitable weigh function is able to identify the risky points of Tsai-Hill criterion. Thus, Local Geary's c is another method to predict the risky points, and it has less equation and does not take a long time for creating the program.

References

[1] L. Liu, J. Yu., L. Cheng. and X. Yang, "Biodegradability of poly (butylenes succinate) (PBS) composite reinforced with jute fiber", Polymer Degradation and Stability, 94 (2009), pp.90-94.

[2] S. Alix, S. Marais, C. Morvan, L. Lebrun, "Biocomposite materials from flax plants: Preparation and properties", Composites: Part A, 39 (2008), pp.1793-1801.

[3] P. Lodha and A. N. Netravali, "Characterization of stearic acid modified soy protein isolate resin and ramie fiber reinforced 'green' composites", Composites Science and Technology, 65 (2005), pp.1211-1225.

[4] S. Serizawa, K. Inoue and M. Iji, "Kenaf-fiber-reinforced poly (lactic acid) used for electronic products", Journal of Applied Polymer Science, 100 (2006), pp.618-624.

[5] A. Gomes, T. Matsuo, K. Goda and J. Ohgi, "Development and effect of alkali treatment on tensile properties of curaua fiber green composites", Composites, Part A, 38 (2007), pp.1811-1820.

[6] LINEO FLAXTAPE© (http://www.lineo.eu/#!products)

[7] H.M. Hsiao and I.M. Daniel 'Elastic properties of composite with fiber waviness', Elsevier Science Limited 1996, pp.931-941.

[8] G. Karami and M. Garnich, "Effective moduli and failure considerations for composites with periodic fiber waviness", Composite Structures, volume 67(2005), pp. 461-475.

[9] B. Ren, K. Goda and J. Noda, "Effects of fiber orientation angles and fluctuation on the stiffness and strength of sliver-based green composites", Journal of the Society of Materials Science, Japan, 59 (2010), pp.567-574.

[10] B. Ren, T. Mizue, K. Goda and J. Noda, "Effects of fluctuation of fibre orientation on tensile properties of flax sliver-reinforced green composites", Composite Structures, 94 (2012), pp. 3457-3464.

[11] Marie-Josee Fortin and Mark Dale, "Spatial Analysis", Cambridge University Press, pp.124-126.

[12] "Flax slivers", Teikokusen-I Co. Ltd., Tokyo, Japan. (http://www.teisen.co.jp)

[13] "Randy PL-1000", Miyoshi Oil and Fat Co. Ltd., Tokyo, Japan. (http://www.miyoshi-yushi.co.jp)

[14] B. Ren, J. Noda, K. Goda, Zairyo/Journal of the Society of Materials Science, Japan, 59-7, (2010), pp. 567-574.

[15] Edited by Ning Hu, Composites and Their Properties, Intech, pp.402-403(2012).

Acknowledgements

I would like to take this opportunity to express my profound gratitude and deep regard to my thesis. This research paper is made possible through the help and support from everyone, including: parents, teachers, family, friends, and in essence, all sentient beings. Especially, please allow me to dedicate my acknowledgment of gratitude toward the following significant advisors and contributors:

First and foremost, I would like to thank Professor Koichi Goda for his most support and encouragement. He kindly read my paper and offered invaluable detailed advices on grammar, organization, and the theme of the paper. I would like to thank Mr. Akira Furuya for helping me in the laboratory and thank Mr. Yin Jie for everything in Japan.

Second, I gratefully acknowledge my finance from the Electric Technology Research Foundation of Chugoku. Especially, I would like to thank Siam University for the scholarship during studying in Japan.

Finally, I sincerely thank to my parents, sister and brother, and colleges at automotive engineering department, Siam University, who provide the advice and support. Especially my wife and my little son, they all kept me going. This research paper would not be possible without all of them.